TECHNICAL MEMORANDUM

588

On the extension of the freak wave warning system and its verification

Peter A.E.M. Janssen and
Jean-Raymond Bidlot

Research Department

May 2009

European Centre for Medium-Range Weather Forecasts
Europäisches Zentrum für mittelfristige Wettervorhersage
Centre européen pour les prévisions météorologiques à moyen

Series: ECMWF Technical Memoranda

A full list of ECMWF Publications can be found on our web site under:
http://www.ecmwf.int/publications/

Contact: library@ecmwf.int

European Centre for Medium-Range Weather Forecasts
Shinfield Park, Reading, RG2 9AX, England

Abstract

This memo discusses a number of updates to the freak wave warning system which were introduced in cycle 33R1 of the IFS. The list of changes is given below and they are discussed in more detail in the remainder of this memo. They are:

1. In shallow water it is well-known that for $kD \simeq 1.363$ the effects of four-wave interactions vanish because of the generation of a wave-induced current. Following the work of Janssen and Onorato (2007), a parametrization of this shallow water effect is introduced which affects both the time evolution of the wave spectrum, and the determination of the kurtosis of the wave field.
2. Extension of the ECMWF freak wave warning system to two-dimensional propagation. Numerical simulations and experimental evidence suggest that the kurtosis of the surface elevation then depends on two parameters, namely the Benjamin-Feir Index (BFI) and a parameter which measures the importance of directional width compared to the width of the frequency spectrum.
3. Introduction of two extreme wave parameters, namely the average maximum wave height and the corresponding wave period. Following the work of Mori and Janssen (2006) it is suggested to use the maximum wave height, observed during a period of length T as an indicator of how extreme the sea state is. For known probability distribution of the sea surface elevation it is shown how to obtain an estimate of the average maximum wave height.

A fairly extensive validation of products of the freak wave warning system is also presented, in particular regarding the maximum wave height. A comparison of the expected maximum wave height against buoy observations shows a good agreement, while also the theoretical probability distribution function of maximum wave height matches the observed distribution very well, in particular in the extremes.

1 Introduction.

Recently, there has been considerable progress in the understanding of the occurrence of freak waves. The notion of freak waves was first introduced by Draper (1965). Freak waves are waves that are extremely unlikely as judged by the Rayleigh distribution of wave heights (Dean, 1990). In practice this means that when one studies wave records of a finite length (say of 10-20 min), a wave is considered to be a freak wave if the wave height H (defined as the distance from crest to trough) exceeds the significant wave height H_S by a factor 2. It should be clear that it is hard to collect evidence on such extreme wave phenomena because they occur so rarely. Nevertheless, observational evidence from time series collected over the past decade does suggest that for large surface elevations the probability distribution for the surface elevation may deviate substantially from the one that follows from linear theory with random phase, namely the Gaussian distribution (cf. e.g. Wolfram and Linfoot, 2000). Also, there are now a number of recorded cases which show that the ratio of maximum wave height and significant wave height may be as large as three (Stansell, 2005).

The increased understanding of the generation of freak waves follows from the present-day ability to simulate these extreme events by means of the Zakharov equation (Zakharov, 1968, Janssen, 2003 (hereafter referred to as J2003)). This is an approximate evolution equation which is obtained from the exact equations for surface gravity waves in the limit of small wave steepness. Yasuda *et al* (1992), Trulsen and Dysthe (1997) and Osborne et al (2000) studied simplified versions of the Zakharov equation and it was found that these waves can be produced by nonlinear self modulation of a slowly varying wave train. An example of nonlinear modulation or focussing is the instability of a uniform narrow-band wave train to side-band perturbations. This instability, known as the side-band, modulational or Benjamin-Feir (1967) instability, will result in focusing of wave energy in space and/or time as is illustrated by the experiments of Lake et al (1977).

Therefore, in the context of the deterministic approach to wave evolution there seems to be a reasonable theoretical understanding of why in the open ocean freak waves occur. In ocean wave forecasting practice one follows,

however, a stochastic approach because the phases of the individual waves are unknown. Clearly, in the context of wave forecasting only statements of a probablistic nature can be made. As freak waves imply considerable deviations from the Normal, Gaussian probability distribution function (pdf) of the surface elevation, the main question therefore is whether the pdf of the surface elevation can be determined in a reliable manner. Following and extending J2003 this is indeed possible. Traditionally, it is known that the surface elevation pdf deviates from the Normal distribution because the actual shape of the ocean waves deviates from the sinusoidal form (this is reflected by the canonical transformation applied to the hamiltonian for water waves (Janssen, 2008). However, there is also a dynamical cause for deviations from Normality. J2003 showed that the deviations from the Normal pdf of the surface elevation are also related to the presence of resonant and nonresonant four-wave interactions. In fact, the kurtosis, which vanishes for a Gaussian distribution and is a measure for extreme events, was found to be related to a six-dimensional integral involving the action density to the third power.

As a first step towards validation of Janssen's approach, the kurtosis was evaluated from the theoretical expression and for uni-directional, narrow-band spectra it was found that the dynamical part of the kurtosis depends on the square of the Benjamin-Feir Index (BFI). Here, the BFI is the ratio of the wave steepness to the spectral bandwidth. This dependence on the BFI was confirmed by recent experimental work done by Onorato *et al* (2005) in the Trondheim wave tank.

For operational implementation the expression for the kurtosis is far too involved, and clearly some simplification is desirable. It is assumed that freak wave events most likely only occur for narrow band wave trains. This corresponds to situations where both the frequency and angular distribution of the waves is narrow. In the narrow-band approximation it is possible to simplify and evaluate the six-dimensional integral. In the present operational system, the dependence on angular width was ignored, resulting in an expression for the kurtosis which depends on the square of the BFI. However, from experimental evidence (Waseda, 2006; Onorato *et al.*, 2009) and numerical simulations (Onorato and Mori, private communication 2006) it is known that kurtosis also depends in a sensitive manner on the angular width. Therefore, in this memo an extension of the kurtosis calculation is presented, and the sensitive dependence on the angular width is confirmed. In fact, it is found that when the relative angular width is larger than $\sqrt{2}$ times the relative frequency width, the sea state is in a defocussing state and extreme waves are less likely to occur than normal. In the opposite case focussing is found. Therefore, for almost uni-directional waves with a large BFI freak waves are most likely to occur, in agreement with the evidence from numerical simulations and wave tanks.

The general result for the kurtosis and its relation to the wave spectrum was originally derived for deep-water waves, but Janssen and Onorato (2007) have shown how to extend it to shallow water. For narrow-band spectra, it is then straightforward to parametrize the stabilizing effects of shallow water.

2 Nonlinear transfer in shallow water.

Finite-amplitude deep-water waves are subject to modulational instability which results in a nonlinear energy transfer among the components in the wave spectrum, which eventually can lead to the formation of extreme waves. However, in shallow water, finite-amplitude surface gravity waves generate a current and deviations from the mean surface elevation. This stabilizes the modulational instability, and as a consequence, in a fairly wide range around $kD = 1.363$ the nonlinear transfer becomes small. In addition, while for $kh > 1.363$ there is nonlinear focussing giving the possibility of the formation of extreme waves, in the opposite case the process of nonlinear focussing ceases to exist. This is a well-known property of surface gravity waves.

Janssen and Onorato (2007) have discussed the consequences of the generation of a wave-induced current for the evolution of the waves spectrum. Due to resonant four-wave interactions the rate of change of the action

density spectrum $N = gF(\mathbf{k})/\omega$ (where F is the wave variance spectrum) is given by

$$\frac{\partial}{\partial t}N_4 = 4\int \mathrm{d}\mathbf{k}_{1,2,3} T^2_{1,2,3,4}\delta(\mathbf{k}_1+\mathbf{k}_2-\mathbf{k}_3-\mathbf{k}_4)R_i(\Delta\omega,t)\left[N_1N_2(N_3+N_4)-N_3N_4(N_1+N_2)\right], \quad (1)$$

where for resonant waves $R_i(\Delta\omega,t) = \pi\delta(\omega_1+\omega_2-\omega_3-\omega_4)$ and $T_{1,2,3,4}$ is a known interaction coefficient. For wave forecasting purposes the evaluation of this three dimensional integral is too time consuming and in practice the Direct-Interaction Approximation (DIA) of Hasselmann *et al* (1985) is used. In the direct interaction approximation the strength of the nonlinear interactions is estimated using the narrow-band approximation of Eq. (1). Hence, in DIA the nonlinear interactions scale with the scaling factor S given by

$$S = \frac{k^2 T^2_{0,0,0,0}}{|\omega_0''|},$$

where ω_0'' is the second derivative of angular frequency with respect to wavenumber k. The second derivative stems from the delta-function for the frequencies in the limit of a narrow-band spectrum. For surface gravity waves on water of finite depth D the dispersion relation reads

$$\omega_0 = \sqrt{gk_0T_0},\ T_0 = \tanh x,\ x = k_0D, \quad (2)$$

while the first and second derivative become

$$v_g = \omega_0' = \frac{1}{2}c_0\left\{1+\frac{2x}{\sinh 2x}\right\},\ c_0 = \frac{\omega_0}{k_0}, \quad (3)$$

and

$$\omega_0'' = -\frac{g}{4\omega_0k_0T_0}\times\Omega'', \quad (4)$$

with

$$\Omega'' = \left\{T_0 - x\left(1-T_0^2\right)\right\}^2 + 4x^2T_0^2\left(1-T_0^2\right). \quad (5)$$

Note that for any value of the depth D the second derivative is always negative. Finally, the narrow-band limit of the interaction coefficient is given by

$$T_{0,0,0,0}/k_0^3 = X_{nl} = \frac{9T_0^4-10T_0^2+9}{8T_0^3} - \frac{1}{k_0D}\left\{\frac{(2v_g-c_0/2)^2}{c_S^2-v_g^2}+1\right\}. \quad (6)$$

with $c_S = \sqrt{gD}$ which is the shallow water wave velocity. Notice that the interaction coefficient consists of two terms where the first term is connected with the nonlinear dispersion relation for surface gravity waves, while the second term is due to effects of wave-induced current and corresponding changes in the mean sea level. These two terms are of definite sign so they may cancel each other, which, in fact, happens for $x = k_0D = 1.363$. Hence, for intermediate water depth waves the nonlinear interactions are expected to play a relatively minor role. So far this property of the nonlinear transfer has not been incorporated in modern wave prediction models.

It is of interest to study the scaling factor S in the deep water limit first. Then, $T_{0,0,0,0}\to k_0^3$, $\omega_0''\to -g/4k_0\omega_0$, while $\omega_0\to\sqrt{gk_0}$. The scaling factor becomes, apart from a constant,

$$S = \frac{\omega_0^{19}}{g^{10}},$$

which is the usual scaling factor found in the deep-water DIA. In the general case one finds

$$S = \frac{\omega_0 k_0^9}{g} \frac{T_0 X_{nl}^2}{\Omega''}, \tag{7}$$

and as a natural extension of the deep-water DIA towards shallow waters the scaling factor (7) has been introduced into Cy 33R1 of the ECMWF wave model software. This scaling factor will give rise to an expected reduction of the strength of the nonlinear transfer around $k_0 D = 1.363$, which has consequences for the frequency downshift of the spectrum in shallow waters. As discussed in Janssen and Onorato (2007) there are also implications for the determination of the surface elevation kurtosis (and therefore for the generation of extreme events) as for $k_0 D < 1.363$ the nonlinear transfer gives rise to defocussing rather than focussing (as happens in the opposite case of $k_0 D > 1.363$).

3 Extension of freak wave warning system.

Before starting with a detailed calculation of the kurtosis of the sea surface and its dependence on the wave spectrum, it is briefly mentioned that the starting point of ocean waves dynamics is the Hamiltonian formulation of the nonlinear water wave equations. Assuming that the waves are weakly nonlinear and applying a *canonical* transformation which removes most of the contributions by non-resonant interactions, one arrives at the well-known Zakharov equation for the free wave part of the action variable. The properties of the Zakharov equation have been studied in great detail by, for example, Crawford *et al.* (1981) for deep-water waves and by Janssen and Onorato (2007) for shallow-water waves. It describes all the known properties of weakly nonlinear waves in deep and shallow water and is therefore a good starting point for further analysis.

Based on the above theoretical development it should be clear that the expression of the kurtosis of the pdf of the surface elevation consists of two additive contributions. The first one was derived by Janssen (2003) and reflects the effects of resonant and non-resonant four-wave interactions, while the second contribution stems from the canonical tranformation and reflects the contribution from asymmetries in the shape of the waves. However, the contribution of the canonical transformation gives a very lengthy expression of several pages and only for narrow band wave trains its form is known explicitely.[1] First the definition of kurtosis used in this work is introduced. Then the general expression of the contribution to the kurtosis by the dynamics of the waves is presented and the limit of a narrow-band wave train is taken. The total kurtosis then consists of the sum of the 'dynamics' contribution and the 'wave-shape' contribution.

3.1 Kurtosis for narrow-band ocean waves.

There are several definitions of kurtosis possible. Here, it is defined in such a way that it is directly related to the fourth cumulant of the pdf of the surface elevation η. Hence, the kurtosis C_4 is defined as

$$C_4 = \frac{\langle \eta^4 \rangle}{3\langle \eta^2 \rangle^2} - 1. \tag{8}$$

The advantage of this definition of kurtosis (some call it the 'excess' kurtosis) is that for a Gaussian pdf C_4 vanishes since for a Gaussian $\langle \eta^4 \rangle = 3\langle \eta^2 \rangle^2$. Hence, C_4 measures deviations from the Gaussian sea state. In other words, when $C_4 > 0$ the probability of extreme events is higher than expected from the Normal distribution, while when $C_4 < 0$ the probability of extreme events is lower than 'Normal'. On the other hand, as shown

[1] A compact expression for the contribution of the canonical transformation to the kurtosis of the sea surface was only obtained just recently, cf. Janssen (2008).

in Janssen (2004), the four-wave interactions only occur because the fourth cumulant is finite, hence there is a direct connection between the changes in the wave spectrum caused by nonlinear four-wave interactions and extreme sea states.

J2003 obtained an expression for the 'dynamics' part of the kurtosis C_4 in terms of the action density spectrum N (cf. Eq. (29) of J2003). Denoting the variance of the surface elevation by $m_0 = \langle \eta^2 \rangle$, one finds

$$C_4 = \frac{4}{g^2 m_0^2} \int \mathrm{d}\mathbf{k}_{1,2,3,4} T_{1,2,3,4} \delta_{1+2-3-4} \left(\omega_1 \omega_2 \omega_3 \omega_4\right)^{\frac{1}{2}} G(\Delta\omega, t) N_1 N_2 N_3, \tag{9}$$

where the transfer function G is given by

$$G(\Delta\omega, t) = \frac{1 - \cos(\Delta\omega\, t)}{\Delta\omega}. \tag{10}$$

Here, $\Delta\omega = \omega_1 + \omega_2 - \omega_3 - \omega_4$, $T_{1,2,3,4}$ is a complicated, homogeneous function of the four wave numbers $\mathbf{k}_1, \mathbf{k}_2, \mathbf{k}_3, \mathbf{k}_4$ which because of the δ-function enjoy the resonance condition $\mathbf{k}_1 + \mathbf{k}_2 = \mathbf{k}_3 + \mathbf{k}_4$. In addition, the angular frequency $\omega(\mathbf{k})$ obeys the dispersion relation $\omega(\mathbf{k}) = \sqrt{gkT_0}$, with k the magnitude of the wave number vector $\mathbf{k}$ and $T_0 = \tanh(kD)$, where D is the water depth. Here only the deep-water limit, $D \to \infty$, will be discussed. The shallow water extension will be addressed in Section 3.5

Eq. (9) is valid for arbitrary two-dimensional action density spectra. Although, strictly speaking, the determination of the kurtosis involves an eight-dimensional integral in wave number space, the resonance conditions restrict the evaluation to a six-dimensional subspace only. Nevertheless, for operational purposes this is still far too time-consuming and in order to make progress, simplifying assumptions have to be made. Here, the so-called narrow-band approximation is assumed which basically implies almost unidirectional waves that have a sharply peaked frequency spectrum. In practice, around the peak of the spectrum this is a valid approximation.

Define the wavenumber spectrum

$$F(\mathbf{k}) = \frac{\omega N(\mathbf{k})}{g}$$

and perform the integration over $\mathbf{k}_4$, then

$$C_4 = \frac{4g}{m_0^2} \int \mathrm{d}\mathbf{k}_{1,2,3} T_{1,2,3,4} \sqrt{\frac{\omega_4}{\omega_1 \omega_2 \omega_3}}\, G(\Delta\omega, t)\, F_1 F_2 F_3 .14$$

In the next step introduce the frequency spectrum

$$E(\omega, \theta) d\omega d\theta = F(\mathbf{k}) d\mathbf{k},$$

hence,

$$C_4 = \frac{4g}{m_0^2} \int \mathrm{d}\omega_1 \mathrm{d}\omega_2 \mathrm{d}\omega_3 \mathrm{d}\theta_1 \mathrm{d}\theta_2 \mathrm{d}\theta_3 T_{1,2,3,4} \sqrt{\frac{\omega_4}{\omega_1 \omega_2 \omega_3}}\, G(\Delta\omega, t)\, E_1 E_2 E_3. \tag{11}$$

Here,

$$\omega_4 = \Omega(\mathbf{k}_4) = \sqrt{g|\mathbf{k}_1 + \mathbf{k}_2 - \mathbf{k}_3|}.$$

For two-dimensional propagation this becomes

$$\omega_4 = \left\{ (\omega_1^2 + \omega_2^2 - \omega_3^2)^2 + 2\omega_1^2 \omega_2^2 \left[\cos(\theta_1 - \theta_2) - 1\right] - 2\omega_1^2 \omega_3^2 \left[\cos(\theta_1 - \theta_3) - 1\right] \right.$$
$$\left. - 2\omega_2^2 \omega_3^2 \left[\cos(\theta_2 - \theta_3) - 1\right] \right\}^{1/4}.$$

Now the narrow-band approximation is applied, i.e. the spectrum is mainly concentrated at $\omega = \omega_0$ and $\theta = \theta_0$, and falls off rapidly, much faster than the other terms in the integrand of Eq. (11). In that event, the transfer coefficient $T_{1,2,3,4}$ can be approximated by its narrow-band value k_0^3. In addition, ω_4 is approximated. Denoting the width of the frequency spectrum by σ_ω and the angular width by σ_θ one may write for angular frequency and direction

$$\omega_1 = \omega_0(1+\delta_\omega \nu_1),\ \theta_1 = \theta_0 + \delta_\theta \phi_1,$$

where in the narrow-band approximation the parameters δ_ω and δ_θ, defined as

$$\delta_\omega = \frac{\sigma_\omega}{\omega_0},\ \delta_\theta = \sigma_\theta, \tag{12}$$

are small. The angular frequency ω_0 may be defined in several ways. For example, one could take it as the peak frequency. Here, for convenience it is defined by means of the first moment

$$\omega_0 = \int \mathrm{d}\omega \mathrm{d}\theta\ \omega E(\omega,\theta)/m_0.$$

Expanding ω_4 in the small parameters δ_ω and δ_θ one finds up to third order

$$\omega_4 = \omega_0 \left\{ 1 + \delta_\omega(\nu_1+\nu_2-\nu_3) - \delta_\omega^2(\nu_3-\nu_1)(\nu_3-\nu_2) + \frac{1}{2}\delta_\theta^2(\phi_3-\phi_1)(\phi_3-\phi_2) \right\} + \mathscr{O}(\delta^3).$$

As a consequence, the frequency mismatch $\Delta\omega$ becomes

$$\Delta\omega = \delta_\omega^2 \omega_0 \left\{ (\nu_3-\nu_1)(\nu_3-\nu_2) - R(\phi_3-\phi_1)(\phi_3-\phi_2) \right\} + \mathscr{O}(\delta^3), \tag{13}$$

where the parameter R has been introduced which measures the importance of the angular width with respect to the frequency width,

$$R = \frac{1}{2}\frac{\delta_\theta^2}{\delta_\omega^2}.$$

Introducing the integral steepness parameter

$$\varepsilon = k_0\sqrt{m_0}.$$

and applying the narrow-band approximation to C_4 the result becomes

$$C_4^{dyn} = 4\varepsilon^2\omega_0 \int \mathrm{d}\nu_1\mathrm{d}\nu_2\mathrm{d}\nu_3\mathrm{d}\phi_1\mathrm{d}\phi_2\mathrm{d}\phi_3\ G(\Delta\omega,t)\ \hat{E}_1\hat{E}_2\hat{E}_3. \tag{14}$$

where $\Delta\omega$ is given by Eq. (13), and the spectrum E is now regarded as a function of ν and ϕ. Also, the spectrum has been normalised in such a way that $m_0 = 1$, hence $\hat{E}_1 = E(\nu_1,\phi_1)/m_0$.

Eq. (14) is the general expression for the dynamics part of the kurtosis of a narrow-band wave train (for this reason the label '*dyn*' is temporarily added). As explained in the beginning of this section, there is also a contribution due to the asymetrical shape of the waves related to the canonical transformation. For a narrow-band wave train one can write down the canonical transformation explicitely and the resulting kurtosis may be evaluated. As a result one finds (Janssen, 2008)

$$C_4 = C_4^{dyn} + 6\varepsilon^2.$$

Therefore, for a narrow-band wave train the wave-shape contribution to the kurtosis is known in terms of the moments of the spectrum, and it is straightforward to evaluate its contribution.

Concentrate once more on the 'dynamics' contribution. Distinguish now two cases namely short times and large times. In addition, when required, the two-dimensional spectrum is approximated by a Gaussian, i.e.

$$\hat{E}(\nu,\phi) = \frac{1}{2\pi}\, e^{-\frac{1}{2}(\nu^2+\phi^2)}, \tag{15}$$

with

$$\nu = \frac{\omega-\omega_0}{\sigma_\omega},\ \phi = \frac{\theta-\theta_0}{\sigma_\theta} \tag{16}$$

This is for the purposes of nonlinear focussing calculations an adequate approximation of the true spectrum as most of the action occurs near the peak of the spectrum.

3.2 Kurtosis for short times.

For short times the resonance function G behaves as

$$\lim_{t\to 0} G(\Delta\omega,t) = \frac{1}{2}\Delta\omega\, t^2,$$

and the kurtosis becomes

$$C_4 = 2\varepsilon^2\omega_0\, t^2 \int \mathrm{d}\nu_1\mathrm{d}\nu_2\mathrm{d}\nu_3\mathrm{d}\phi_1\mathrm{d}\phi_2\mathrm{d}\phi_3\ \Delta\omega\, \hat{E}_1\hat{E}_2\hat{E}_3.$$

Introducing the dimensionless time τ according to

$$\tau = \omega_0\delta_\omega^2\, t,$$

and making use of the expression for the frequency mismatch, Eq. (13), the kurtosis now becomes

$$C_4 = \tau^2 BFI^2 \int_{-\infty}^{\infty} \mathrm{d}\nu_{1,2,3}\mathrm{d}\phi_{1,2,3}\ \{(\nu_3-\nu_1)(\nu_3-\nu_2) - R(\phi_3-\phi_1)(\phi_3-\phi_2)\}\hat{E}_1\hat{E}_2\hat{E}_3, \tag{17}$$

where BFI is the Benjamin-Feir Index, defined as

$$BFI = \frac{\varepsilon\sqrt{2}}{\delta_\omega}. \tag{18}$$

Note that in the spirit of the narrow-band approximation the integration is taken from $-\infty$ to ∞ which introduces an error which is exponentially small. For short times it is seen that apart from a quadratic dependence on dimensionless time τ the kurtosis depends on two dimensionless parameters, namely the Benjamin-Feir Index and the parameter R which measures the importance of directional width. More qualitative statements can be made by evaluating the integral in Eq. (17). One immediately finds for arbitrary narrow-band spectra the simple result

$$C_4 = \tau^2 BFI^2\,(1-R)\,.$$

since, thanks to the use of the mean frequency ω_0 as a typical frequency, by definition integrals involving odd powers in ν and/or ϕ vanish.

This result clearly shows that directional effects play an important role as depending on the size of R there is even an initial evolution towards negative kurtosis, resulting in defocussing rather than focussing. In other words, when $\delta_\theta < \sqrt{2}\delta_\omega$ kurtosis is positive corresponding to nonlinear focussing and hence an increased probability of extreme waves , while for large angular width ($\delta_\theta > \sqrt{2}\delta_\omega$) kurtosis is negative and extreme waves occur less likely than 'Normal'.

3.3 Kurtosis for large times.

For large times the resonance function G behaves as

$$\lim_{t\to\infty} G(\Delta\omega,t) = \frac{\mathscr{P}}{\Delta\omega}, \tag{19}$$

where the symbol $\mathscr{P}$ denotes the principle value integral. The integral contains a singularity at $\Delta\omega = 0$ and the principle value simply means that one makes in the integration contour a cut of size 2ε around the singularity in a symmetrical fashion and the limit $\varepsilon \to 0$ is taken afterwards.

Using (19) the kurtosis becomes

$$C_4 = 4\varepsilon^2\omega_0\mathscr{P}\int \mathrm{d}\nu_1\mathrm{d}\nu_2\mathrm{d}\nu_3\mathrm{d}\phi_1\mathrm{d}\phi_2\mathrm{d}\phi_3\ \frac{\hat{E}_1\hat{E}_2\hat{E}_3}{\Delta\omega}.$$

Substitution of the expression for the frequency mismatch (13) gives

$$C_4 = 2BFI^2\mathscr{P}\int_{-\infty}^{\infty}\mathrm{d}\nu_{1,2,3}\mathrm{d}\phi_{1,2,3}\ \frac{\hat{E}_1\hat{E}_2\hat{E}_3}{(\nu_3-\nu_1)(\nu_3-\nu_2)-R(\phi_3-\phi_1)(\phi_3-\phi_2)}. \tag{20}$$

Not much progress has been made with this general expression for the kurtosis of narrow-band waves. The only general result found thus far assumes that the spectrum has the same form in frequency and direction, i.e. $\hat{E}(\nu_1,\phi_1) = \hat{E}(\phi_1,\nu_1)$. Under this condition it can be shown by means of interchanging integration variables ($\nu_1 \leftrightarrow \phi_1$, etc) that the following relation holds for C_4:

$$C_4(BFI,R) = -\frac{1}{R}C_4(BFI,\frac{1}{R}). \tag{21}$$

This is a powerful relation because once one knows C_4 for $R<1$, Eq. (21) immediately gives the kurtosis for $R>1$. Clearly, once more it is seen that $R=1$ plays, just as in the short time limit a special role. Substituting $R=1$ in (21) one immediately finds that C_4 vanishes,

$$C_4(BFI,R=1) = 0. \tag{22}$$

It can also be shown that at $R=1$ the kurtosis C_4 must change sign.[2] Therefore, depending on the value of R there will be nonlinear focussing ($C_4>0$) or nonlinear defocussing ($C_4<0$).

The integral in (20) has been evaluated for the special case of the Gaussian spectrum (15) in Appendix A. To good approximation it is found that

$$C_4 = J(R)\ BFI^2, \tag{23}$$

where for $R<1$

$$J(R) = \frac{1}{(2\pi)^2}\frac{1-R}{R+R_0}, \tag{24}$$

with $R_0 = 3\sqrt{3}/4\pi^3$, while $J(R)$ for $R>1$ follows from relation (21).

Eqns. (23-24) show that for large times the kurtosis depends on the square of the BFI and on the ratio of directional width and frequency width through the parameter R. Just as in the short time limit and in agreement with Eq. (22) kurtosis is seen to vanish for $R=1$.

[2] The argument for this so far goes as follows, and it holds for symmetrical spectra: If R vanishes then (15) will have a certain sign, while for large R it will have the opposite sign. This suggests a change of sign somewhere in the R-domain. For symmetrical spectra the only candidate so far is $R=1$.

3.4 Nonlinear Schrödinger Equation simulations.

In the previous section an expression for the large time value of the kurtosis was obtained for stationary spectra. However, the assumption that the spectrum does not change in time is not always correct as was found out when Onorato and Mori (private communication, 2006) did $\pm 20,000$ simulations with the Nonlinear Schrödinger Equation (which follows from the narrow-band limit of the Zakharov equation). In particular, when $R > 1$ initially, hence the frequency width smaller than the directional width, there are due to the Benjamin-Feir Instability rapid changes (broadening in the frequency direction) such that in the course of time the kurtosis flips from negative to positive. This property is illustrated in Fig. 1 where for simulations of the two-dimensional NLS equation over a fixed time interval of 100 periods the maximum of the kurtosis as function of BFI and δ_θ is shown suggesting that the maximum is always positive.

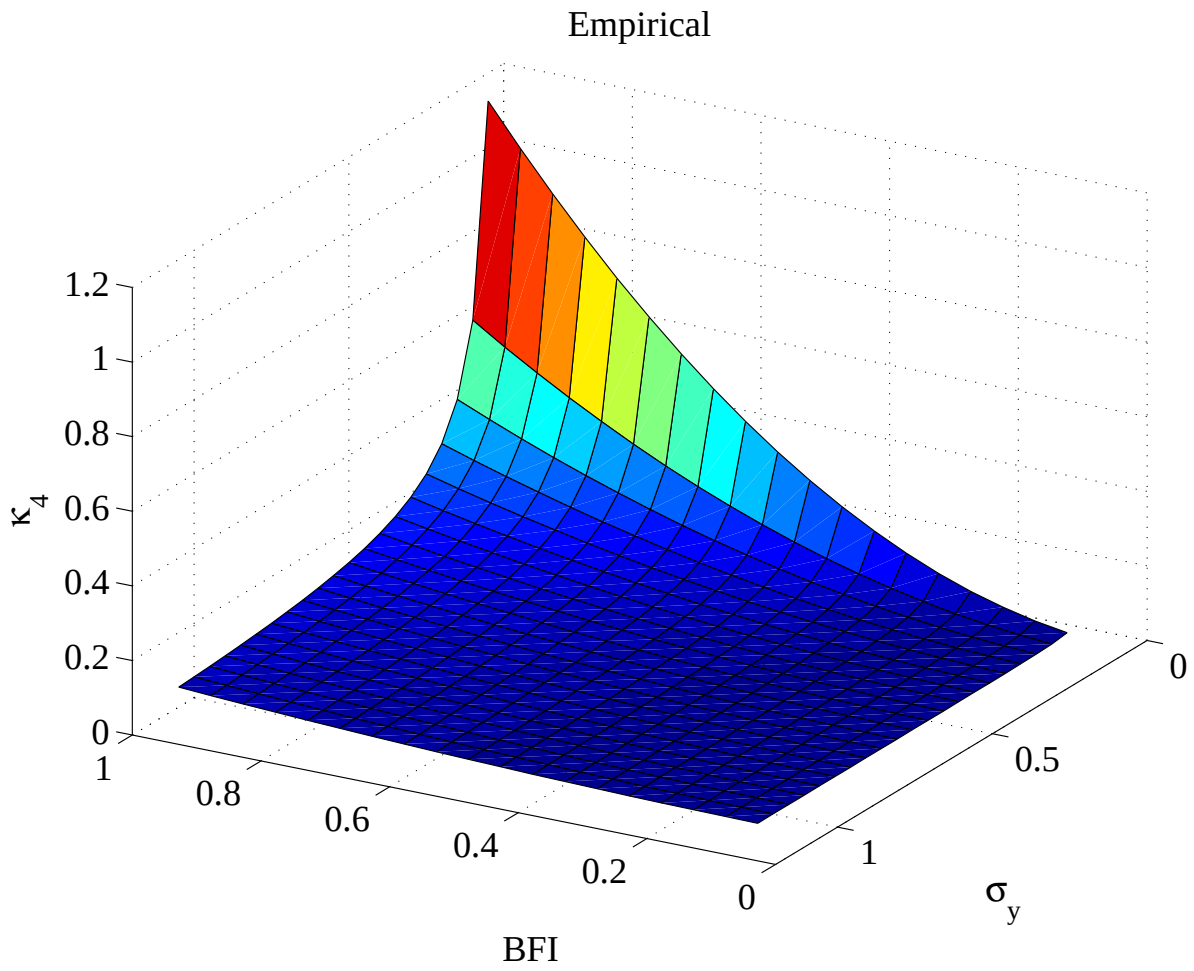

Figure 1: Maximum kurtosis C_4 as function of BFI and of dimensionless angular width δ_θ.

3.5 Operational Implementation of kurtosis calculation.

Based on the numerical evidence displayed in Fig. 1 N. Mori found the following fit for the maximum of the kurtosis

$$C_4^{dyn} = \frac{0.031}{\delta_\theta} \times \frac{\pi}{3\sqrt{3}} BFI^2, \tag{25}$$

therefore, finite directional width δ_θ is seen to give a considerable reduction in kurtosis C_4^{dyn}. Including the contribution from the shape of the waves the total kurtosis becomes now

$$C_4 = C_4^{dyn} + \alpha\varepsilon^2. \tag{26}$$

where for deep-water $\alpha = 6$.

This result holds for deep-water waves. The extension to shallow water is achieved by means of a redefinition of the Benjamin-Feir Index.[3] Recall (see J2003) that this dimensionless parameter just expresses the balance between nonlinearity and dispersion. For the general, shallow- water case this gives a new parameter which is called B_S. It is defined as (Janssen and Onorato, 2007)

$$B_S^2 = -BFI^2 \times \left(\frac{v_g}{c_0}\right)^2 \frac{gX_{nl}}{k\omega_0\omega_0''}, \tag{27}$$

where the relevant symbols are defined in Eqns. (2)-(6) and BFI is given by Eq. (18). The extension of the kurtosis calculation towards shallow water is now simply achieved by replacing in Eq. (25) BFI^2 by B_S^2. Note that in the deep-water limit it can readily be shown that the second part of the expression for B_S^2 becomes -1, therefore in this limit B_S^2 reduces to the usual definition for the BFI, cf. Eq. (18). Studying now the dependence of B_S^2 on depth it is seen that for decreasing dimensionless depth k_0D the square of the Benjamin-Feir index is slowly decreasing until around $k_0D = 1.363$ when there is a rapid transition from positive to negative values. Hence for $k_0D < 1.363$ the kurtosis may become negative which implies that there are less extreme events than the norm, while in the opposite case there are more frequent extreme events.

3.5.1 Determination of the BFI and δ_θ.

The estimation of the Benjamin-Feir Index requires knowledge of the significant steepness ε and the spectral width δ_ω in frequency space. In addition, an estimate of the directional width δ_θ is required as well. Here, a description is given of a robust method to estimate the BFI for modelled and observed spectra, which was introduced in cycle 26R3 of the IFS. In particular, the estimation of the width of observed frequency spectra is not a trivial task, because observed spectra show considerable noisy behaviour around the peak of the spectrum (which is frequently ill-defined).

Janssen and Bouws (1986) have developed a robust method to estimate the width of observed spectra, which was applied to frequency spectra obtained from a waverider located at IJmuiden over a fifteen year period. Following Goda these authors used the peakedness factor Q_p defined as

$$Q_p = \frac{2}{m_0^2} \int_{\mathscr{D}} \mathrm{d}\omega\ \omega E^2(\omega)$$

where Janssen and Bouws (1986) chose, after extensive experimentation, as integration domain $\mathscr{D}$ all frequencies for which $E(\omega) > 0.25E(\omega_p)$. However, in cycle 26R3 $\mathscr{D}$ was taken over all frequencies, because this

[3] Also the parameter α needs adjustment for the shallow water case, but this has not been introduced yet

was thought to be more robust . The advantage of this integral measure is that, because of the dependence on the square of the frequency spectrum, peaks in the spectrum are emphasized. Janssen and Bouws (1986) also explored alternative integral measures such as one based on the second moment of the wave spectrum, but these alternatives give more emphasis to the high-frequency part of the spectrum and are therefore more sensitive to high-frequency noise.

In the kurtosis calculation of the previous section it has been assumed that around the peak the spectrum has a Gaussian shape (15), and therefore it makes sense to evaluate Q_p also for a Gaussian. In fact, Janssen and Bouws (1986) checked from the observed spectra that to a good approximation the spectra are symmetrical around the peak and that the Gaussian approximates the observed spectral shape well. In the narrow-band approximation one finds to high accuracy

$$Q_p = \frac{1}{\delta_\omega \sqrt{\pi}} \tag{28}$$

where δ_ω is the relative width defined in Eq. (12). A robust method to estimate the relative spectral width now is to determine the spectral Q_p and to invert Eq. (28), hence

$$\delta_{\omega,obs} = \frac{1}{Q_{p,obs}\sqrt{\pi}}$$

As a consequence, the observed BFI becomes

$$BFI = k_0 m_0^{1/2} Q_{p,obs} \sqrt{2\pi}$$

The modelled BFI is calculated in an identical fashion through the peakedness factor Q_p and the integral steepness ε. However, further inspection of the results shows that for simple JONSWAP spectra the procedure overestimates the width of the frequency spectrum. For example for a young windsea case with overshoot parameter $\gamma \simeq 3.3$ the procedure underestimates the value of the BFI by a factor of two. In cycle 33R1 it was therefore decided to restrict the integration domain of Q_p to the peak region, by reverting back to the original approach of Janssen and Bouws (1986), and this restriction in the domain alleviates the underestimation problem with the BFI.

The directional width δ_θ at the peak of the spectrum may be estimated by the usual approach, i.e.

$$\delta_\theta = \sqrt{2(1-M_1)}$$

where $M_1 = I_1/m_0$ and $I_1 = \int \mathrm{d}\omega \mathrm{d}\theta \cos(\theta) E(\omega,\theta)$, but it won't always provide the sharpest estimate of directional width near the peak.

An alternative approach to estimation of the frequency and directional width of the two-dimensional model spectrum is to fit the one-dimensional frequency and directional spectra with a parabola thus giving sharp estimates for δ_ω and δ_θ. In fitting the parabola also a sharper estimate of the peak period T_p may be provided as up to now the peak period did correspond to the maximum of the one-dimensional frequency spectrum so T_p could only assume discrete values because of the discretization of the wave spectrum in frequency space. However, occasionally the fitting procedure may fail because, e.g., the peak of the spectrum is erratic. Therefore from cycle 33R1 and onwards the widths are determined by taking the minimum value from the integral method, i.e. Q_p and M_1, and from the fitting procedure. Nevertheless, because of the relatively coarse discretization of the spectrum, narrow spectra are too wide in the present version of the ECWAM model. To accomodate for this, the constant has been increased in the expression for the kurtosis, Eq. (25), by a factor of two from 0.031 to 0.062.

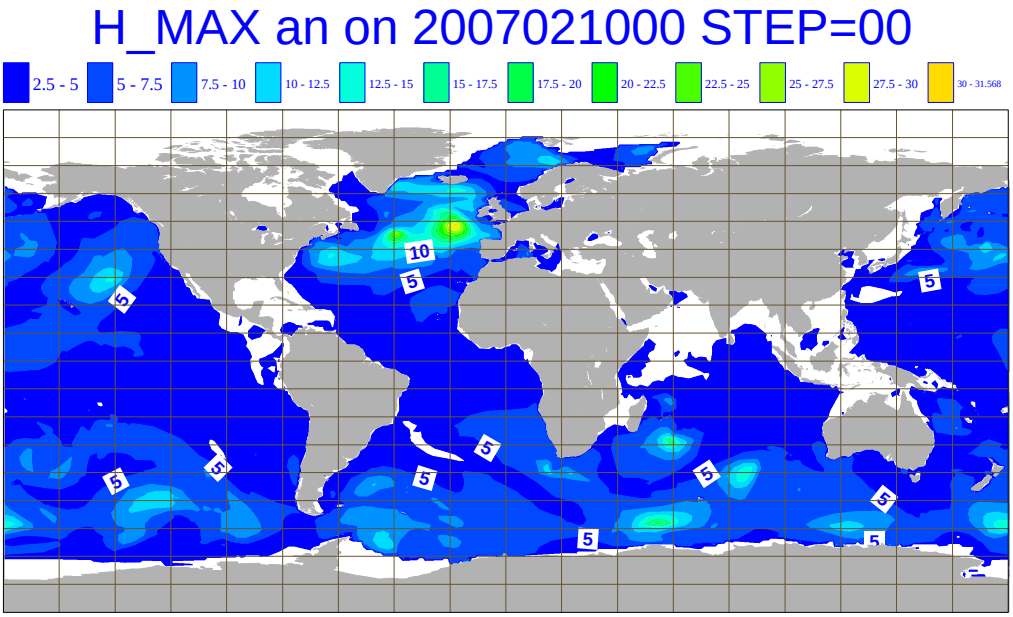

Figure 2: Map of analyzed maximum wave height for the 10^{th} *of February 2007.*

4 Maximum wave height and period.

In this memo a simple measure for extreme sea states will be introduced. It is common to define as a freak wave a wave whose height is at least 2.2 times the significant wave height. This is a very discrete and singular approach, which is in practice not easy to verify. Nevertheless, it is desirable to be able to quantify extreme sea states and to be able to validate them against observations in a meaningful manner. It is then natural to consider the concept of maximum wave height, a concept which is well-known in engineering practice. It should be realized, as also pointed out extensively by Mori and Janssen (2006), that the maximum waveheight H_{max} not only depends on the shape of the probability distribution function of the sea surface, but also on the number of waves at hand. Consider now a time series of wave heights of length T involving a number of N waves. A good estimate of the maximum wave height is the expectation value for maximum wave height denoted by $\langle H_{max} \rangle$. As an extension of Goda's work for Gaussian sea states, $\langle H_{max} \rangle$ will be determined for a pdf with finite kurtosis and the result will be compared with observations of maximum wave height from buoys. The agreement is good, and therefore this measure for maximum wave height has been introduced into the operational ECMWF wave forecasting system.

Before proceeding it is mentioned that there is an important caveat. It is well-known that for narrow-band wave trains the probability density function (pdf) of wave height is the Rayleigh distribution. This was shown a long time ago by Longuet-Higgins (e.g. 1957). He noted that it is in general straightforward to obtain the statistical properties of the envelope of a wave train, even for broad-band wave trains. For a Gaussian sea state the pdf of the envelope is found to be the Rayleigh distribution. The statistical properties of waveheight are much harder to obtain. For narrow-band wave trains it can be argued that waveheight is twice the envelope and thus wave height will then follow the Rayleigh distribution as well. However, for broad-banded wave trains the pdf of wave height is not known.

One may wonder why it is so difficult to obtain the pdf of wave height for general spectra of finite width. An important reason for this is that, at least in a theoretical context, wave height is an *ill-defined* quantity, in contrast to, for example, the envelope of a wave train. Analyzing a time series it is fairly easy (see for example Appendix B) to construct at any point in time the envelope of a wave train, however, this is not possible for the wave height

of a wave train (except of course in the narrow-band approximation). In practice, researchers obtain the wave height distribution by means of the zero-crossing method. This is a very elegant method, which is easily implemented: Search for two consecutive zero-upcrossings in the time series and determine the wave height from the difference of the maximum and the minimum of the surface elevation η in the corresponding time interval. Thus, wave height is determined by sampling with the zero-crossing frequency $(m_2/m_0)^{1/2}$ (with m_n the n^{th} moment of the wave spectrum). However, what about sampling with other frequencies, corresponding to different (spatial) scales. For higher sampling frequency, wave heights are expected to be reduced compared to lower sampling frequency because one would expect that at smaller scales wave heights are smaller. Therefore wave height depends on the choice of spatial and temporal scale, and hence the wave height pdf will depend on the way one samples the time series.

For the envelope distribution there is much less of a problem, because the envelope is a continuous function of time. By sampling at a sufficiently high frequency one simply gets the 'usual' pdf for envelope. In fact, in the Appendix B a review of the derivation of the pdf of the envelope is given and it will be shown that for linear waves the pdf is always Rayleigh, despite claims by Longuet-Higgins (1983) to the contrary. This derivation is based on the joint probability distribution of envelope and period, which does depend on spectral width, but the marginal distribution law for the envelope can be shown to be independent of the spectral width parameter $\nu^2 = m_0 m_2/m_1^2 - 1$. In addition it will be shown that this theoretical joint pdf is in perfect accord with the one obtained from numerical simulations of the surface elevation for a Gaussian sea state.

Finally, one may wonder why one is interested so much more in the waveheight distribution rather than the envelope probabilities. If one is interested in extreme forces on structures such as oil riggs or ships than one would expect that the quantity of interest is something like the energy of the waves, which is closely related to the square of the envelope. For extreme cases the square of the wave height would underestimate the force on structures (as the pdf of wave height falls below the Rayleigh distribution, while the pdf of the envelope is Rayleigh). In other words, there is a case to concentrate on the envelope distribution rather than the wave height distribution. Alternative arguments to use the envelope rather than wave height are presented in Longuet-Higgins (1984).

Therefore, the theoretical developments will all concern the (statistical) properties of the envelope of a wave train and wave height is defined as twice the envelope. Details of the theoretical development and its verification against Monte Carlo simulations are presented in Appendix B. In order to obtain an expression for the expection value of maximum wave height the work of Mori and Janssen (2006) is followed closely. One may then take the following steps

1. Start from the pdf of surface elevation η, which is the well-known Gram-Charlier expansion, i.e. pdf depends on skewness and kurtosis, which are assumed to be small.

2. Obtain the pdf of 'wave height' defined as twice the envelope. Here the envelope ρ follows implicitely by writing the surface elevation signal as

$$\eta = \rho \cos\phi$$

with ϕ the local phase of the wave train. Local wave height is then defined as $H = 2\rho$ and the wave height distribution in terms of wave height normalized with the significant wave height becomes:

$$p(H) = 4H \exp(-2H^2)\,[1 + C_4 A_H(H)] \tag{29}$$

where

$$A_H(H) = 2H^4 - 4H^2 + 1$$

Note that because of symmetries the pdf of H does not contain skewness.

3. The maximum wave height distribution is obtained by simply writing down the probability that for given number of independent waves N the maximum wave height has a certain chosen value. The maximum wave height distribution $p_m(H_{max})$ becomes

$$p_m(H_{max}) = N\left[1 - P(H_{max})\right]^{N-1} p(H_{max})$$

where, with $B_H(H) = 2H^2\left(H^2-1\right)$,

$$P(H) = \int_H^\infty \mathrm{d}h\; p(h) = \exp(-2H^2)\left(1 + C_4 B_H(H)\right)$$

is the exceedence probability of wave height, N is the number of waves, and $p(H_{max})$ follows from Eq. (29). In the continuum limit this becomes

$$p_m(H_{max}) = N p(H_{max}) \times \exp\left[-NP(H_{max})\right] \tag{30}$$

Notice that the maximum wave height distribution involves a double exponential function.

4. The expectation value of maximum wave height follows from

$$\langle H_{max}\rangle = \int_0^\infty \mathrm{d}H_{max}\, H_{max}\; p_m(H_{max}) \tag{31}$$

Notice that $H_{max} = F[C_4(BFI,R),N]$, where $N = T_D/T_p$ with T_p the peak period and T_D the duration of the timeseries. By making this choice for the number of waves N it is tacitly assumed that two successive 'waves' are uncorrelated. This assumption is hard to justify because the correlation between two following waves may be of the order of 50 %. It would be more appropriate to correct for this correlation thereby either reducing the number of degrees of freedom or reducing the variance of the pdf.

The integral in (31) may be evaluated in an approximate fashion for large N and small C_4. Details of this calculation are given in Appendix C. The main result becomes

$$\langle H_{max}\rangle = \sqrt{\langle z\rangle}, \tag{32}$$

where

$$\langle z\rangle = \hat{z}_0 + \frac{\gamma}{2} + \frac{1}{2}\log\left[1 + C_4\left\{2\hat{z}_0(\hat{z}_0-1) - \gamma(1-2\hat{z}_0) - \frac{1}{2}(\gamma^2 + \frac{\pi^2}{6})\right\}\right], \tag{33}$$

with $\hat{z}_0 = \frac{1}{2}\log N$ and $\gamma = 0.5772$ is Euler's constant. An estimate of the sharpness of the estimate for the expectation value of maximum wave height may be given as well. This follows immediately from the width σ of the maximum wave height distribution. For linear waves its width σ is approximately (see Appendix C for the details)

$$\frac{\sigma}{\langle H_{max}\rangle} \simeq \frac{\pi}{2\sqrt{6}\left(\log N + \frac{1}{2}\gamma\right)}, \tag{34}$$

and clearly, the longer the time series of independent events, the sharper the estimate for maximum wave height becomes.

Next it is discussed how the corresponding maximum period was obtained. As reported in Appendix B, so far only the case of linear waves has been worked out, so this still requires extension into the nonlinear regime. The period is estimated using the joint pdf of normalized envelope,

$$R = \frac{\rho}{\sqrt{2m_0}},$$

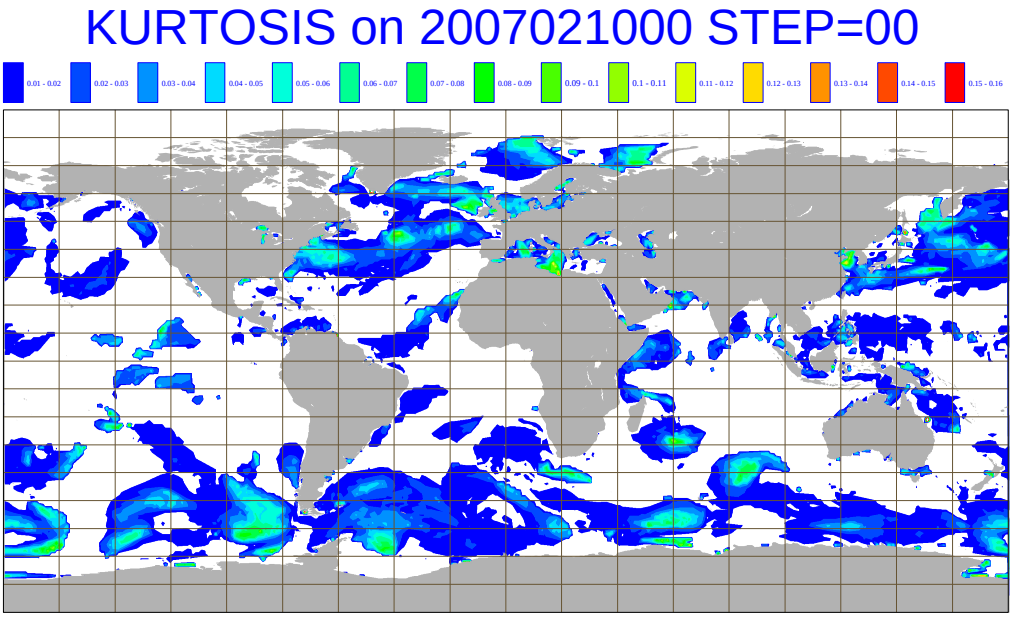

Figure 3: Map of analyzed kurtosis C_4 for the 10^{th} of February 2007.

and normalized period

$$T = \frac{\tau}{\overline{\tau}},$$

where the period $\tau = 2\pi/\omega = -2\pi/\dot{\phi}$, and the mean period $\overline{\tau} = 2\pi m_0/m_1$. This joint pdf reads

$$p(R,T) = \frac{2}{\nu\pi^{1/2}}\frac{R^2}{T^2}\exp\left\{-R^2\left[1+\frac{1}{\nu^2}\left(1-\frac{1}{T}\right)^2\right]\right\},$$

where ν is the width parameter as introduced by Longuet-Higgins (1983),

$$\nu = (m_0 m_2/m_1^2 - 1)^{1/2}.$$

For given normalized envelope height wave period follows from the conditional distribution of wave periods $p(T|R) = p(R,T)/p(R)$, or,

$$p(T|R) = \frac{R}{\nu\pi^{1/2}T^2}\exp\left[-\frac{R^2}{\nu^2}\left(1-\frac{1}{T}\right)^2\right],$$

The expectation value of the period then becomes

$$\langle T\rangle = \frac{R}{\nu\pi^{1/2}}\int_{-\infty}^{\infty}\frac{\mathrm{d}T}{T}\exp\left[-\frac{R^2}{\nu^2}\left(1-\frac{1}{T}\right)^2\right].$$

Introducing the parameter $\Delta = \nu/R$ the above integral may be evaluated for small Δ in an approximate fashion with the result

$$\langle T\rangle = 1+\frac{1}{2}\Delta^2+\frac{3}{4}\Delta^4+\ldots,$$

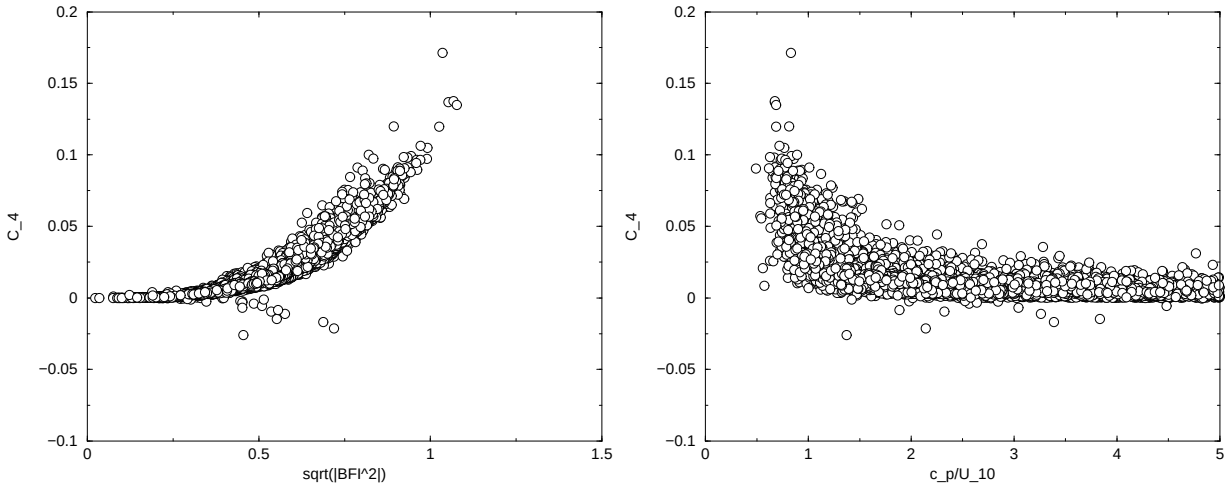

Figure 4: The left panel shows the dependence of kurtosis C_4 on the Benjamin-Feir Index, while the right panel shows the dependence of C_4 on the wave age parameter c_p/U_{10}.

and the maximum period then follows from $\tau_{max} = \overline{\tau}\langle T \rangle$. Finally, the small parameter Δ involves the ratio of ν and $R = R_{max}$. While ν follows in a straightforward fashion from the first three moments of the wave spectrum, R_{max} requires knowledge of the value of the envelope at the extreme. Explicitely,

$$R_{max} = \sqrt{2}\frac{H_{max}}{H_S}.$$

Let us now discuss some characteristic properties of the new freak wave warning system. In Fig. 2 an example of a maximum wave height map is shown for a big storm in the North Atlantic that occurred on the 10^{th} of February 2007. Here, the maximum wave height refers to time series with a duration T_D of 3 hrs and the number of waves N follows from the relation $N = T_D/T_p$, where T_p is the peak period. The maximum of significant wave height in the North Atlantic was 15.9 m at that time while the extremum in maximum wave height is found to be 31.6 m. Notice, however, the dependence of the estimate of the maximum wave height on the number of waves in the time series of duration T_D. Although according to Eq. (33) it only depends on the logarithm of N, nevertheless for $T_D = 20$ min maximum wave height will decrease on average by about 20% giving an extreme value of 26.5 m. Inspecting the kurtosis map shown in Fig. 3, however, it is found that regarding maximum wave height, the extreme event in the North Atlantic was not exceptional as the kurtosis C_4 was only about 0.06 corresponding to a normalized maximum wave height H_{max}/H_S of only 1.95. In order to appreciate that such a condition is not exceptional the left panel of Fig. 4 shows the relation between C_4 and BFI obtained from the global field at 2007021000 UTC. For display purposes the original 0.5° field was subsampled to 1.5°. Typically, maximum values of kurtosis are around 0.2 at values of BFI of the order 1. It is also of interest to study under what kind of meteorological conditions exceptional waves may occur. Some information on this is provided by the right panel of Fig. 4, which shows kurtosis plotted against the wave age parameter c_p/U_{10}. In particular for young windsea with $c_p/U_{10} < 1$ large values of kurtosis, and hence abnormal sea states, are possible according to the present approach. Young windseas typically occur in fetch-limited conditions, when the wind just start blowing or during the passage of a front when the wind turns by a significant amount.

According to Eqns. (32)-(33) the normalised maximum wave height depends on two parameters namely the number of waves N and the kurtosis parameter C_4. Fig. 5 shows the dependence of kurtosis on these two parameters as obtained from the global field of Fig. 2. In particular, the figure in the right panel, which

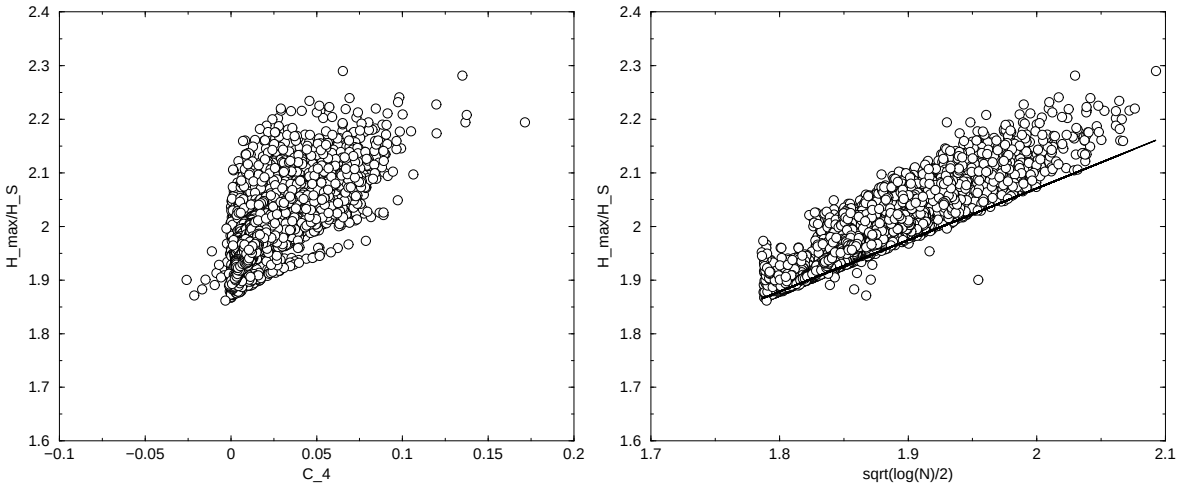

Figure 5: The left panel shows the kurtosis dependence of the expectation value of normalised maximum wave height $\langle H_{max} \rangle$ while the right panel shows the dependence of $\langle H_{max} \rangle$ on the number of waves N in the timeseries of duration of 3 hrs through the parameter $\sqrt{\log N/2}$. The full line shows the relation between H_{max} and the number of waves for vanishing kurtosis.

shows normalised maximum wave height as function of $\sqrt{\log N/2}$, is illuminating. A comparison with the corresponding relation for vanishing kurtosis immediately shows the importance of nonlinearity on the estimate of maximum wave height. While for this synoptic case the full line never meets the criterium for freak waves to occur (recall the condition for freak waves is $H_{max}/H_S > 2.2$), when effects of nonlinearity through a finite value of kurtosis are included there *are* a number of cases that meet the criterion for extreme events. The question now is how realistic is the ECMWF freak wave warning system.

4.1 Verification aspects and maximum wave height verification.

It is clear that for operational applications a choice for the length of the timeseries needs to be made. Buoy time series are typically 20-30 minutes long so initially it was thought that, in order to validate the model results against buoy data, it would make sense to take this period as the length of the time series. However, for practical application a timescale related to the changes in the synoptic conditions seems more appropriate. This would mean a much longer duration of say 3 hrs. A compromise was found by choosing a duration of 3 hrs, while for validation purposes 6 consecutive buoy observations were collected making up an observed duration of about 3 hrs. The observed maximum wave height is then the maximum of the 6 consecutive maximum wave height observations.

In the data set currently used in the ECMWF wave verification system (Bidlot *et al.*, 2005; Bidlot *et al.*, 2007) only Canada (Meds) and Norway (Oceanor) supply buoy observations of maximum waveheight. Inspecting the distributions for normalised maximum wave height of MEDS buoys and Oceanor buoys it was found that they belong to two different populations: the mean value of normalised maximum wave height of the Oceanor buoys was considerably smaller than the mean value from the MEDS buoys. It is suspected that this is related to a different length of the time series used (17.5 min. (Oceanor) versus 30 min. (MEDS)) and possibly to a different procedure to obtain an estimate of maximum wave height. Because the majority of maximum wave height measurements is from MEDS, only the latter data will be considered for the validation of the probability

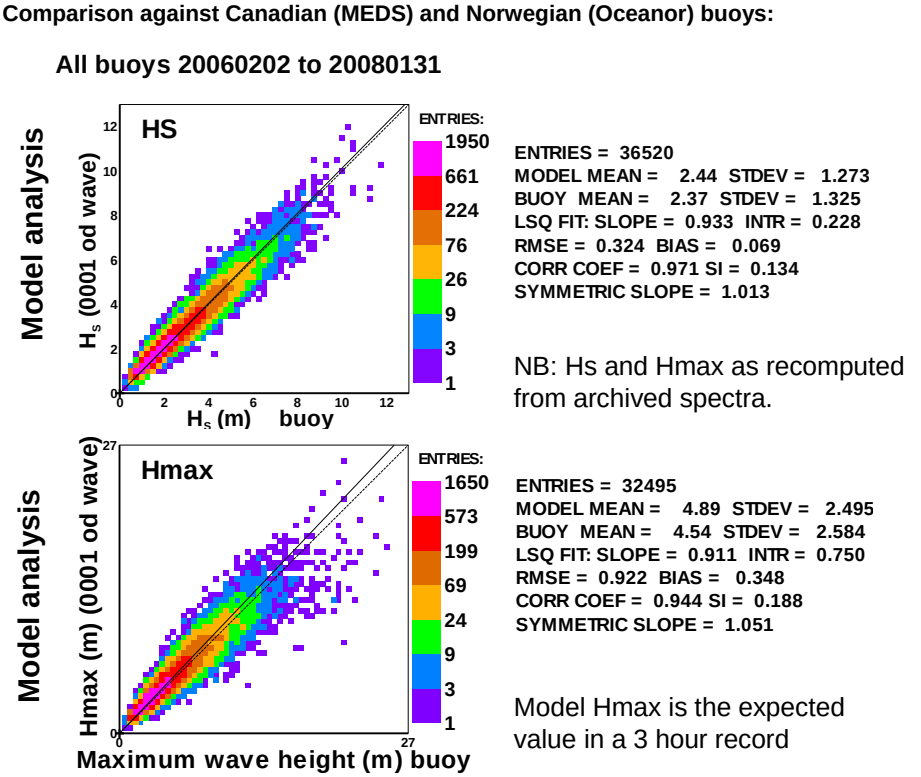

Figure 6: Validation of analyzed maximum wave against observed maximum wave height from a number of buoys that report maximum wave height (the buoy list is shown as well). Period is February 2006 until January 2008. For a comparison of the quality of the H_{max} estimates the validation of model wave height against buoy data is shown as well.

distribution function, although for the verification of maximum wave height all data will be used.[4] The MEDS buoys have a single accelerometer and the maximum wave height is obtained by taking twice the maximum of a surface elevation timeseries obtained at all the times where acceleration is minimal. This procedure does not give the maximum of envelope wave height but there is no other routinely observed information on maxima available. Nevertheless, this may give rise to problems in the interpretation of the comparison between model and observations.

First results of a comparison of modelled and observed maximum wave height are shown in Fig. 6. For a first comparison the agreement between modelled and observed maximum wave height is quite impressive. The relative positive bias is about 5% while the scatter index is about 19%. For comparison the scatter index for significant wave height for the same set of buoys and period is about 13%. This impressive agreement is puzzling, because for starters actually apples and pears are being compared, since the model value is an expectation while the buoy value is instantaneous. This puzzle was solved when it was realized that the pdf of maximum wave height is fairly narrow. For linear waves its width σ is approximately given by Eq. (34). Clearly, the longer the length of the time series the sharper the estimate of maximum wave height becomes. For

[4]The MEDS data have the additional advantage that also one-dimensional spectra are reported. These are needed later to determine the *BFI*.

a 3 hour duration and a peak period of 10 s one finds $\sigma/\langle H_{max}\rangle \simeq 0.08$, therefore the maximum wave height distribution is indeed fairly narrow as the scatter index has the much larger value of 19%.

4.2 Verification of the probability density function.

Nevertheless, it is emphasized that apples and pears *are* being compared. This is clearly visible in the plot of the geophysical[5] distribution of normalised (by significant wave height) expectation value and a comparison with the graph of the distribution of the actual, observed value of the normalised maximum wave height, as shown in the left panel of Fig. 7. The width of the modelled maximum wave height distribution, being about 0.05, is much smaller than the width of the observed distribution, which is about 0.16 and it is evident that there is no resemblance between the two distributions. The reason for this discrepancy is most likely that the observed distribution is a single realisation which is not necessarily representative for the area of interest, while the modelled distibution is based on the expectation value of the normalised maximum wave height.

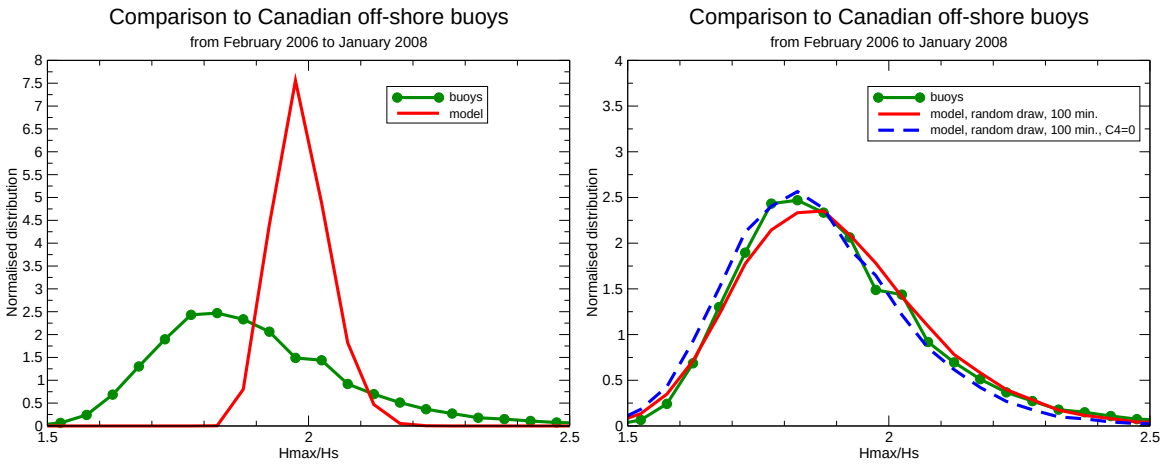

Figure 7: The left panel shows the comparison between observed H_{max}/H_S distribution and the modelled distribution of the expected normalised maximum wave height. The right panel shows in stead of the distribution of the expected maximum wave height the model distribution obtained by a random draw of H_{max} for given number of waves and given kurtosis. The right panel also shows the impact of nonlinearity on the maximum wave height distribution by means of a plot of the case of zero kurtosis. The length of the timeseries is 100 min. which is thought to match the length of the buoy time series.

The question now arises whether it is possible to simulate the observed distribution of normalised maximum wave height. This turns out to be possible indeed and in order to understand the method that will be followed, it is important to return to the basic mechanism of freak wave generation. As already discussed in the Introduction freak waves are regarded to be the result of a nonlinear focussing phenomenon but it should be realized, as pointed out in J2003, that the focussing is the most efficient when the phases of the waves involved in the focussing are chosen appropriately (constructive interference). However, in the field there is no knowledge of the phases and for practical purposes the phases are chosen in an *almost* random manner. Nonlinearity will give rise to a certain degree of correlation between the waves and for this reason the adjective almost, and the effects

[5]There is a need now to make a distinction between the maximum wave height pdf and the geophysical distribution of maximum wave height. In principle the geophysical distribution follows from the combination of the maximum wave height pdf and the geophysical distribution of the number of waves N and the kurtosis C_4. Only when the latter distributions are much more narrow than the maximum wave height pdf the geophysical distribution will coincide with the maximum wave height pdf. For brevity the adjective geophysical will be dropped

of small nonlinearity on the pdf are given in Eqns. (29) and (30).

A way to simulate the observed distribution of maximum waveheight is therefore to start from the theoretical pdf of maximum wave height (30), the explicit form of which is given in Eq. (C1), and to generate from this pdf for given number of waves N and given kurtosis C_4 a random draw of normalised maximum wave height. The usual procedure for this is detailed in Appendix C and basically one obtains a random draw of maximum waveheight from the condition that the cumulative distribution is a random number between 0 and 1. For duration a 100 min period has been chosen as this is thought to match the length of the buoy time series appropriately, despite the fact that according to the data provider the length of the time series is 30 min. [6] The resulting modelled distribution function is plotted in the right panel of Fig. 7 and the very good agreement with the observed distribution is to be noted, in particular in the extremes. For reference, also the model distribution according to linear theory (i.e. $C_4 = 0$) is plotted and although linear theory gives a reasonable agreement with the observations it is noted that extremes are underestimated by linear theory. This underestimation of the extremes has some practical consequences. It is common to define a freak wave as an event with $H_{max}/H_S > 2.2$. Integrating the nonlinear and the linear distribution from 2.2 until infinity one finds that according to linear theory 4.5% of the cases are freak wave events while according nonlinear theory 7.5% of the cases are freak waves which amounts to an increase of 60%. According to the observations 8.5% of the cases are freak waves, therefore nonlinear theory underestimates the number of freak waves somewhat.

The slight underestimation by nonlinear theory is more pronounced when a plot of the logarithm of the distribution is made as shown in Fig. 8 and is compared to the logarithm of the observed distribution.[7] It is evident

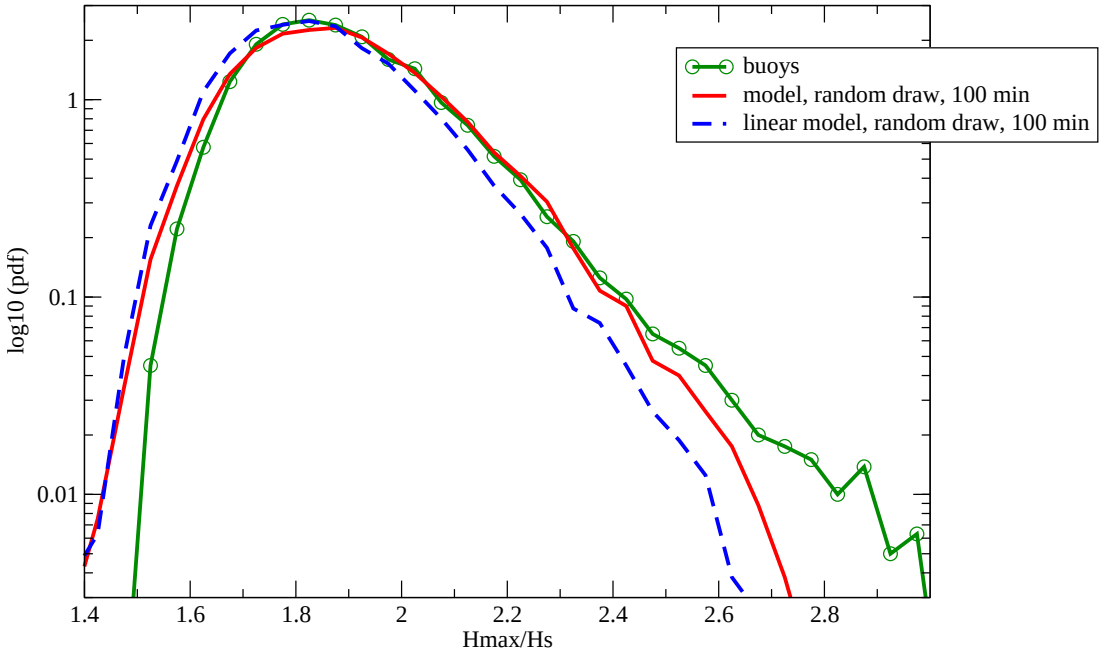

Figure 8: The logarithm of maximum wave height distribution obtained by a random draw of H_{max} for given number of waves and given kurtosis as compared to the observed maximum wave height distribution.

[6] Note that according to Fig. 6 the model overestimates maximum wave height by 5%. This overestimation can be removed by reducing the number of degrees of freedom N or equivalently by shortening the length of the timeseries from 180 min. to 100 min. This reduction in the number of degrees of freedom is in qualitative agreement with the correlation between two successive waves.

[7] This comparison was restricted to cases with a significant wave height larger than 2 m because buoys might have problems with accurately representing low sea states. This is also evident in the next section where buoys are not representing high frequencies very well. This reduces the number of collocations from 32,000 to 16,000. Nevertheless there are still about 1,300 cases that satisfy the freak wave criterion of $H_{max}/H_S > 2.2$

that the really extreme events with $H_{max}/H_S > 2.5$ are seriously underestimated by the present nonlinear theory, although in the range of 1.9 until 2.5 there is good agreement. The reason for the discrepancy between model and observations is not clear at present. Noting that this is a first, preliminary comparison a number of detailed studies of the buoy time series need to be carried out. A first look at the time series for maximum wave height suggests that these really extreme events are present only for a very short time. However, at present there is no criterion to decide whether these cases can be regarded as outliers or not. Also, the buoys are giving maximum wave height based on twice the crest value which may be an overestimate of envelope wave height. On the other hand, the discrepancy for very extreme normalised maximum wave heights may also be an indication that the Gram-Charlier expansion for the pdf of the surface elevation is not adequate for these extremes. This is further discussed at the end of this section. In Fig. 8 also the logarithm of the pdf according to linear theory has been plotted and it is suggested that linear theory underestimates the extremes to a considerable extent, as differences with the observations start already at $H_{max}/H_S = 2$.

The estimate for the number of freak waves can also be obtained in an analytical manner. A straightforward integration of the pdf on maximum wave height from $z_c^{1/2} = H_{max}/H_S = 2.2$ to infinity gives

$$J = \int_{H_{max}=2.2}^{\infty} dH_{max}\; p_m(H_{max}) = 1 - \exp\left[-Ne^{-2z_c}\left(1 + C_4 B(z_c)\right)\right], \tag{35}$$

where $B(z) = 2z(z-1)$. Although the number of waves N is fairly large, typically $N = \mathcal{O}(1000)$, the criterion for a freak wave, $z_c = 2.2^2$, is such that e^{-2z_c} is tiny so that the product Ne^{-2z_c} may be regarded as small. In that event the first exponential in (35) may be replaced by its argument and to a good approximation one finds

$$J = Ne^{-2z_c}\left(1 + C_4 B(z_c)\right).$$

The above expression gives the number of freak waves for a particular realization. In order to be able to relate this to the geophysical results displayed in Fig. 7 and 8 the ensemble average is taken. As a priori a correlation between the number of waves and the nonlinearity of the wave field is not expected it is found that $\langle NC_4\rangle = \langle N\rangle\langle C_4\rangle$ [8] and therefore the ensemble average of J becomes

$$\langle J\rangle = \langle N\rangle e^{-2z_c}\left(1 + \langle C_4\rangle B(z_c)\right).$$

For the present synoptic case it is found that for a 100 minute time window $\langle N\rangle = 593$ while $\langle C_4\rangle = 0.021$ only. As a consequence, including finite kurtosis effects one finds that the number of freak waves is 6.6% while according to linear theory the number of freak waves is only 3.7%, hence nonlinearity increases the number of freak waves by 70%. Note that these results are in close agreement with the results from Fig. 7. Although the average value of the kurtosis is small it is multiplied by $B(z_c) = \mathcal{O}(40)$ which is fairly big, therefore even small nonlinear effects may have a significant impact on the number of freak waves.

Finally it is remarked that also for the pdf itself it is of interest to obtain the average pdf over the geophysical distribution. For the extreme states the surprising result is then obtained that the tail of the distribution depends on the average value of kurtosis. This is surprising because most researchers would expect that the tail of the distribution is determined by the extreme values of the kurtosis. In order to understand this a bit better consider the pdf of maximum wave height, given in Eq. (C1), and consider the limit of extreme values of normalised maximum wave height $y = H_{max}/H_S$. Then the pdf of maximum wave height is approximately

$$p_m(y) \approx 4Nye^{-2y^2}\left[1 + C_4 A_H(y)\right],\; y >> 1, \tag{36}$$

in other words, for extreme values the pdf of maximum wave height is apart from the factor N just given by wave height distribution (29). Clearly, the geophysical ensemble average of p_m depends on the average value of the

[8] In fact this assumption can immediately be checked using the present synoptic condition. One finds $\langle (N - \langle N\rangle)(C_4 - \langle C_4\rangle)\rangle / (\langle N\rangle\langle C_4\rangle) \approx 0.1$ which is small enough so that the assumption of decorrelation applies.

kurtosis C_4 and not on the extreme values. Apparently the effects of the random draw are overwhelming. Most cases encountered have a small value of kurtosis, but because of the random draw there is a finite probability that a large value of normalised maximum wave height is obtained. The contribution by the small kurtosis cases apparently dominates the one from the large kurtosis cases even in the tail of the geophysical distribution of maximum wave height. Therefore, strictly speaking the present model for extreme waves has not yet been validated for large values of the kurtosis.

Furthermore, Eq. (36) shows that in essence the tail of the maximum wave height distribution is given by the wave height distribution which follows in a straightforward fashion from the Gram-Charlier expansion of the surface elevation pdf. Although the tail of the observed distribution function is exponential, an inspection of (36) reveals that for large values of normalised maximum wave height the model pdf drops off faster, suggesting that the Gram-Charlier expansion may be problematic in this very extreme range with $y > 2.5$. The shape of the wave height pdf has shown good agreement with observations from a wave tank for example, but the very extreme range with $y > 2.5$ has never been validated.

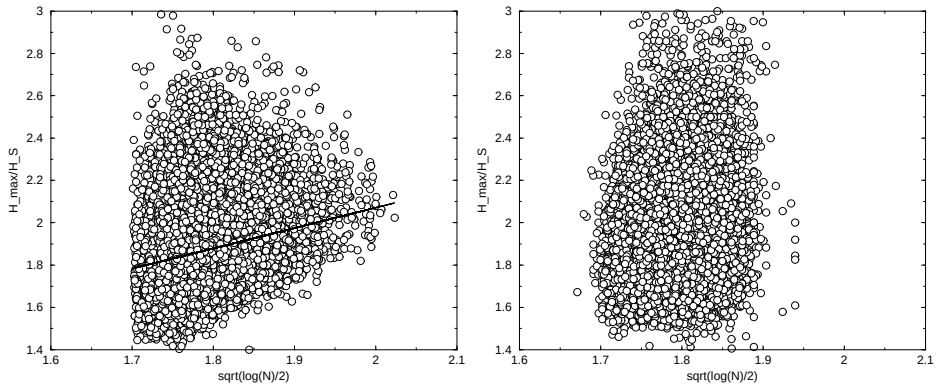

Figure 9: The left Panel shows the dependence of H_{max}/H_S, obtained as a random draw from the pdf (30), on the number of waves N in the timeseries of duration of 100 min through the parameter $\sqrt{\log N/2}$. The full line shows the relation between expected H_{max} and the number of waves for vanishing kurtosis. The right Panel shows the corresponding scatter diagram as found from the buoy observations.

4.3 Finding empirical relations.

It is concluded from the above discussion that the statistics of observed extreme waves may be well simulated by using kurtosis and the number of waves from our wave forecasting system, provided the normalised maximum wave height is drawn in a random manner from the theoretical pdf (30). This implies that using our approach it is possible to simulate how certain observed relations or scatter diagrams will look like. A prominent example is the relation between maximum wave height and the number of waves. Ignoring nonlinear effects for the moment one would expect, based on Eqns. (32)-(33) a definite relation between the expectation value of normalised wave height and the number of waves since $\langle H_{max} \rangle = ((\log N + \gamma)/2)^{1/2}$, and even in the presence of nonlinearity there seems to be a reasonable correlation between the two as follows from the right panel of Fig. 5. Randomness, however, seems to destroy such a relation. In order to show this the scatter plot of the right panel of Fig. 5 was redone, but now using a random draw of maximum wave height. The result is given in the left panel of Fig 9 and compared with Fig. 5 there is a considerable increase in scatter. This also follows from a linear fit to the data, as for the expectation value of maximum wave height a correlation of 92% is found while the random draw only gives a correlation of 30%. The observations, shown in the right panel, give a similar

scatter, but evidently high frequencies ($\approx 0.5Hz$), corresponding to $(\log N/2)^{1/2} \approx 2$, are under represented by the buoy data. Presumably this is because buoys are insensitive to these high frequencies.

From this large drop in correlation it follows that it will be extremely difficult to try to obtain empirical relations from observations. An exception is perhaps the validation of maximum wave height against observations as shown in Fig. 6. Using a random draw of maximum wave height the scatter index only increases from 19% to 22%, apparently because the scatter of the random noise is small compared to the scatter index itself.

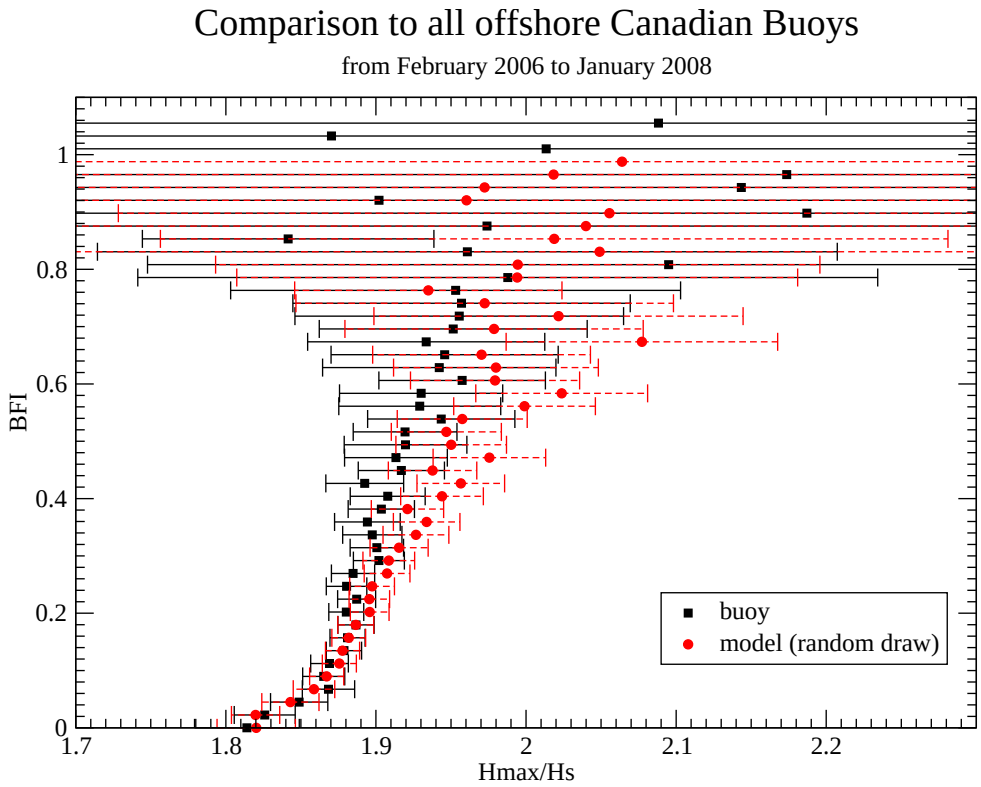

Figure 10: Dependence of observed H_{max}/H_S on observed Benjamin-Feir Index. Modelled random draw of normalised maximum wave height (based on timeseries of 3 hrs which are reduced in length by 40 %) against the Benjamin-Feir Index is shown as well. The error bars are an indication of the error in normalised maximum wave height.

Alternatively one may perform a careful averaging of the data to reduce the effects of randomness. Burgers *et al.* (2008) collected in the order of 2 years of observations of the ratio H_{max}/H_S obtained from AUK platform in the central North Sea and collocated these observations with archived values of the BFI from the ECMWF model. Their results suggest that there may indeed a relation between normalised maximum wave height and a spectral shape parameter such as the BFI. Their work was redone using the present data set. The present results are given in Fig. 10. Here, observed normalised maximum wave height against observed BFI[9] (black squares) is plotted, while for comparison purposes also the corresponding model relation between the average of a random draw of normalised maximum wave height and the average BFI (red squares) is shown. A similar average relation is found when the expectation value of maximum wave height is taken but the error bars are much smaller. The present results are in agreement with Burgers *et al.* (2008). The plot seems to confirm that the model for extreme sea states even gives reasonable results for fairly extreme values of the BFI and the kurtosis.

Finally, it is emphasized that Fig. 10 only gives an indication that the normalised maximum wave height

[9] as determined from the observed one-dimensional spectra using the integral method of §3.6

depends on some nonlinear aspects of the sea state. As a proxy for nonlinearity the BFI was used. However, inspecting the model for the kurtosis given in Eq. (26), the situation is somewhat more complicated. It is evident that parameters such as the wave steepness ε and the directional width δ_θ are important as well. Furthermore, the observations of H_{max} are obtained from the maximum crest, which implies that observations should also depend on the skewness.

5 Conclusions.

This report describes an update of the ECMWF freak wave warning system and its first, still preliminary validation against observations of maximum wave height. This version became operational in June 2008.

The freak wave warning system has been extended by including effects of directionality in the estimation of the kurtosis of the surface elevation pdf, while also the contribution of bound waves to the kurtosis has been introduced. Furthermore, a parametrisation of shallow water effects in the kurtosis calculation has been introduced. Next, we two new output parameters have been discussed, namely maximum wave height and the corresponding period, which provide some simple measures for extreme sea states. The maximum wave height pdf, which includes nonlinear effects, was obtained following the work of Mori and Janssen (2006).

A preliminary extensive validation of the maximum wave height product was performed as well. The present system is capable of giving realistic estimates of extreme ocean wave events. However, because of the nature of these events, only probablistic statements can be issued. This is evident from the validation of the modelled maximum wave height distribution function against individual observed events as a random draw from the theoretical pdf was required in order to get a good match with the observed pdf.

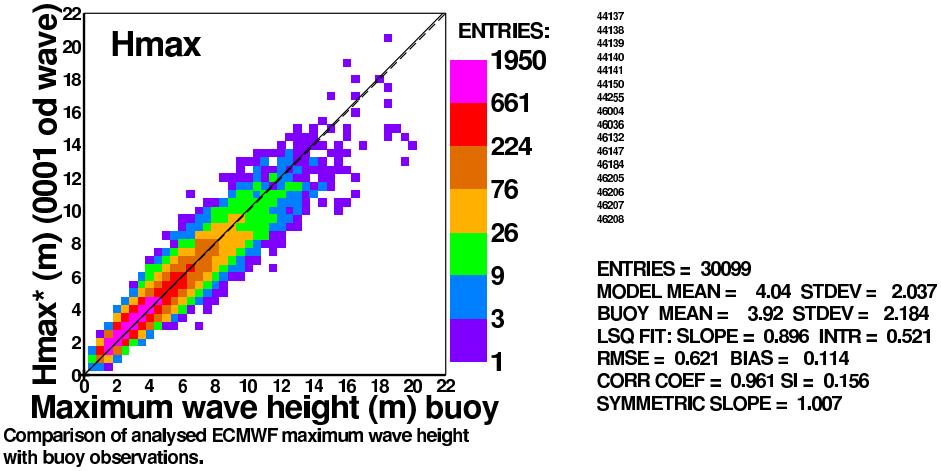

Figure 11: Comparison of observed and modelled expectation value of maximum wave height. Time interval for the model pdf is 18 mins, consistent with a 40 % reduction of the number of degrees of freedom. Period is February 2006 until January 2008.

The main output of the warning system is the expectation value of maximum wave height over a three hour time interval. Unfortunately, we cannot validate the quality of this parameter as no observations of the expectation value over a three hour interval are available to us. Nevertheless, one can make the compromise to consider the expectation value of normalised maximum wave height over the much shorter period of 30 mins. The observed estimate for the expectation value of maximum wave height now follows from the average of the 6 successive observations (rather then taking the maximum of the 6 observations as done in section 4.1). Again it is suspected that correlation effects are relevant and therefore the number of degrees of freedom in the model

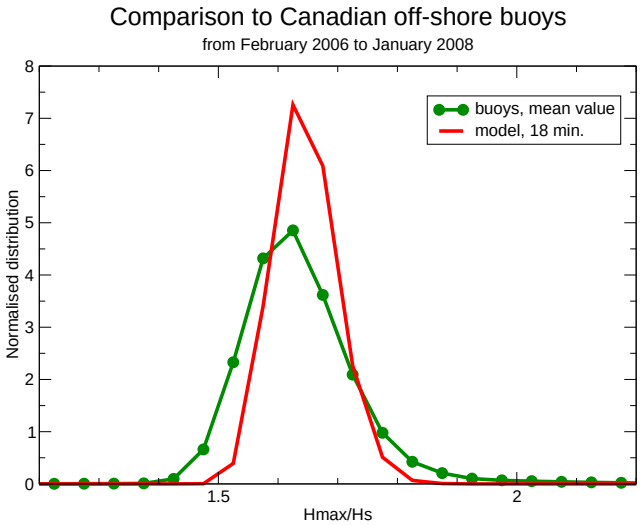

Figure 12: Comparison of observed and modelled expectation value of normalised maximum wave height distribution. The model time interval is 18 mins.

pdf is reduced by 40%. This choice provides an unbiased estimate of modelled maximum wave height. The resulting comparison between modelled and observed maximum wave height is shown in Fig. 11 while the comparison between modelled and observed geophysical distribution of normalised maximum wave height is shown in Fig. 12. Again for the much shorter time series there is a good agreement between modelled and observed maximum wave height, while, as expected, the averaging procedure applied to the observations results in a much sharper geophysical distribution function. No doubt, if there would have been more independent observations available at the relevant synoptic times this would have resulted in a even sharper distribution function. Therefore, the expectation value of maximum wave height over the shorter time interval seems to be a valuable product, and by extrapolation it is expected that the same holds true for the present operational product, which is the expectation value of maximum wave height over a three hour interval.

For a first validation, it is believed that some promising results have been obtained. Nevertheless, a number of issues need to be clarified. For example, the effects of correlation between successive waves on the probability distribution function of maximum wave height have to be estimated. Presently it is assumed that two wave events are not correlated, but this assumption is hard to justify as the correlation between two successive waves may be of the order of 50 %. However, to estimate effects of correlation is not a trivial task. A first step was taken by Kimura (1980) and Longuet-Higgins (1984) who, following the work of Uhlenbeck (1943) and Rice (1945), studied the joint probability distribution $p(\rho_1, \rho_2)$ of the envelope ρ_1 at time t and the envelope ρ_2 at time $t+\tau$ and its dependence on correlation. One of the interesting conclusions from their work is that for finite correlation κ the variance of the pdf, usually given by m_0, is reduced by the factor $\sqrt{1-\kappa^2}$. Although the effect of correlation is only of second order, this still may give a considerable shift in the maximum wave height pdf of the order of $5-10\%$ towards lower normalised maximum wave height. The task to estimate effects of correlation is, unfortunately, nontrivial as the joint pdf of $N-1$ somewhat correlated events is required.

Furthermore, it is required to study in what manner the Gram-Charlier expansion for the pdf of the surface elevation may be extended into the regime of very extreme events. The Gram-Charlier expansion is an expansion of the pdf in terms of the Gaussian distribution and its derivatives. Although this set of basis functions is orthogonal it is by no means certain that this gives a uniformly valid expansion for extreme values. Furthermore, for large values of the kurtosis the pdf may become negative, which is a highly undesirable property of the expansion.

Also, and this is work still in progress, more realistic estimates of the canonical part of the kurtosis need to be

developed. Presently, the narrow-band approximation is used where the canonical part of the kurtosis is given by $6\varepsilon^2$ (see Eq. (26)), but it is already known from Janssen (2008) that for realistic spectra the contribution of bound waves to the kurtosis may increase by a factor of two.

Finally, according to the buoy observations there are freak waves in 8.5% of the cases, while according to nonlinear theory there are freak waves in 7.5 % of the cases. This does not imply, of course, that this is the frequency of "monster waves" as one still needs to multiply this number by the frequency of occurrence of large significant wave height events. Adopting as criterion of an extreme event that significant wave height should be larger than 8 m, then according to the available information from altimeter satellite data and first-guess wave model results the probability that on a global scale significant wave height is larger than 8 m equals 0.003. Therefore, the probability of having "monster waves" somewhere on the globe is about 0.00024.

Appendices.

A Evaluation of Eq. (20).

The integral in (20) is now evaluated for the special case of the Gaussian spectrum (15). Substituting (15) into (20) one finds

$$C_4 = J(R)\, BFI^2,$$

where

$$J(R) = \frac{2}{(2\pi)^3}\mathscr{P}\int_{-\infty}^{\infty} \mathrm{d}\nu_{1,2,3}\mathrm{d}\phi_{1,2,3}\, \frac{e^{-\frac{1}{2}(\nu_1^2+\phi_1^2+\nu_2^2+\phi_2^2+\nu_3^2+\phi_3^3)}}{(\nu_3-\nu_1)(\nu_3-\nu_2)-R(\phi_3-\phi_1)(\phi_3-\phi_2)}$$

Note that the integral contains singularities and is 6-dimensional. This therefore presents a challenge when evaluated on the computer. It was decided to do some analytical work first.

A.1 Step 1.

In the first step it is realized that although the integral is 6-dimensional, the denominator is essentially 4-dimensional as it depends on the difference variables $\nu_3-\nu_1$, $\nu_3-\nu_2$, $\phi_3-\phi_1$, and $\phi_3-\phi_2$ only. Therefore introduce new variables according to

$$x_1 = \frac{\nu_1-\nu_3}{\sqrt{3}},\ x_2 = \frac{\nu_2-\nu_3}{\sqrt{3}},\ \nu_3$$
$$x_3 = \frac{\phi_1-\phi_3}{\sqrt{3}},\ x_4 = \frac{\phi_2-\phi_3}{\sqrt{3}},\ \phi_3$$

and the integration over the variables ν_3 and ϕ_3 can be performed immediately. The eventual result is

$$J(R) = \frac{2}{(2\pi)^2}\mathscr{P}\int_{-\infty}^{\infty} \mathrm{d}x_{1,2,3,4}\, \frac{e^{-(x_1^2+x_2^2-x_1x_2)-(x_3^2+x_4^2-x_3x_4)}}{x_1x_2-Rx_3x_4}$$

which reduces the dimension of the integration by two but the singularities have not yet been removed.

A.2 Step 2.

In the next step introduce polar coordinates, which is always a good idea when dealing with Gaussians. Hence introduce

$$x_1 = \rho_1\cos\theta_1,\ x_2 = \rho_1\sin\theta_2,\ x_3 = \rho_2\cos\theta_2,\ x_4 = \rho_2\sin\theta_2,$$

and introduce the new variables

$$z_1 = \rho_1^2,\ z_2 = \rho_2^2,\ \phi_1 = 2\theta_1,\ \phi_2 = 2\theta_2.$$

The result for J becomes

$$J(R) = \frac{1}{4\pi^2}\int_0^{2\pi}\mathrm{d}\phi_{1,2}\int_0^{\infty}\mathrm{d}z_{1,2}\, \frac{e^{-z_1(1-\frac{1}{2}\sin\phi_1)-z_2(1-\frac{1}{2}\sin\phi_2)}}{z_1\sin\phi_1-Rz_2\sin\phi_2} \tag{A1}$$

hence this involves much simpler exponential functions. In fact, it turns out that the integrations over z_1 and z_2 can be performed. In order to see this introduce the double integral

$$I = \int_0^\infty \frac{\mathrm{d}z_{1,2}}{z_1 - \beta z_2}\, e^{-a_1 z_1 - a_2 z_2},$$

where $a_1 = 1 - \sin\phi_1/2$, $a_2 = 1 - \sin\phi_2/2$, and $\beta = R\sin\phi_2/\sin\phi_1$. Introduce the transformation

$$v = \frac{z_1}{\beta z_2} - 1,$$

then the integral can be rewritten as

$$I = \mathscr{P}\int_{-1}^{\infty} \frac{\mathrm{d}v}{v} \int_0^\infty \mathrm{d}z_2\, e^{-z_2(a_1\beta + a_1\beta v + a_2)},$$

which simplifies the problem considerably because the singularity becomes a fixed point. In addition one may perform immediately the integration over z_2 with the result

$$I = \mathscr{P}\int_{-1}^{\infty} \frac{\mathrm{d}v}{v} \frac{1}{a_2 + \beta a_1 + \beta a_1 v},$$

which is an almost trivial integral over v. Evaluation of the integral gives[10]

$$I = \frac{1}{a_2 + \beta a_1} \log|\frac{a_2}{\beta a_1}|. \tag{A2}$$

The result has an interesting structure because when the denominator vanishes, $a_2 + \beta a_1 \to 0$, at the same time $|a_2/\beta a_1| \to 1$. Hence the logarithm approaches 0 giving for I a finite answer, $I \to -1$. Therefore, the integration over z_1 and z_2 has removed the singularity. Nevertheless, the numerical evaluation has to be done with care. When the denominator is sufficiently small, the appropriate limit for I is taken.

The integral $J(R)$ in (A1) now becomes (making use of the definitions for a_1, a_2 and β),

$$J(R) = \frac{1}{4\pi^2}\int_0^{2\pi} \mathrm{d}\phi_1 \mathrm{d}\phi_2 \;\; f(s_1, s_2, R),$$

where

$$f(s_1, s_2, R) = \frac{1}{s_1(1 - \frac{1}{2}s_2) + Rs_2(1 - \frac{1}{2}s_1)} \log\left|\frac{s_1(1 - \frac{1}{2}s_2)}{Rs_2(1 - \frac{1}{2}s_1)}\right|, \tag{A3}$$

and the notation $s_1 = \sin\phi_1$, and $s_2 = \sin\phi_2$ has been introduced.

A.3 Numerical computation.

Still some development is required, because as (A3) stands, it is not easy to take the limit for small R, because R appears in an awkward manner in the logarithm. Therefore, the integration domain has been splitted in two parts, one from $(0, \pi)$ and one from $(\pi, 2\pi)$. In the last domain a new variable is introduced in such a way that the integration range shifts to $(0, \pi)$. Thus, take $\phi = \theta + \pi$ and as a consequence the sin-function changes sign since $\sin\phi = -\sin\theta$. As a result, $J(R)$ will consist of four contributions involving the function $f(\pm s_1, \pm s_2, R)$

[10] because the integrand is locally an odd function of v the principle value integral will not give a contribution related to the singularity at $v = 0$.

with all combinations of the sign (hence the expression for $J(R)$ becomes invariant for the sign of the sin-function). Finally, the integration domain $(0,\pi)$ is splitted into two domains, namely $(0,\pi/2)$ and $(\pi/2,\pi)$. Applying the transformation $\phi = \pi - \theta$ maps it to the former domain, while $\sin\phi = \sin\theta$. This reduction of the integration domain by a factor of two increases the integrand by a factor of 4. The eventual result is

$$J(R) = \frac{1}{\pi^2}\int_0^{\pi/2} \mathrm{d}\phi_1 \mathrm{d}\phi_2 \left\{ f(+s_1,+s_2) + f(-s_1,-s_2) + f(-s_1,+s_2) + f(+s_1,-s_2) \right\} \tag{A4}$$

where for brevity the dependence on R has been dropped. The result (A4) has the advantage that with the same resolution the numerical evaluation is four times faster. In addition, it is now possible to take the small and large R-limit.

For example, consider the small R-limit. Taking the limit $R \to 0$ before hand in the denominator, the integrand of (A4) becomes

$$\begin{aligned} &+\frac{1}{s_1(1-\frac{1}{2}s_2)}\log\left|\frac{s_1(1-\frac{1}{2}s_2)}{Rs_2(1-\frac{1}{2}s_1)}\right| - \frac{1}{s_1(1+\frac{1}{2}s_2)}\log\left|\frac{s_1(1+\frac{1}{2}s_2)}{Rs_2(1+\frac{1}{2}s_1)}\right| \\ &-\frac{1}{s_1(1-\frac{1}{2}s_2)}\log\left|\frac{s_1(1-\frac{1}{2}s_2)}{Rs_2(1+\frac{1}{2}s_1)}\right| + \frac{1}{s_1(1+\frac{1}{2}s_2)}\log\left|\frac{s_1(1+\frac{1}{2}s_2)}{Rs_2(1-\frac{1}{2}s_1)}\right| \end{aligned}$$

Because of the common front factor the first and the third term may be combined and it is seen that the $\log(1/R)$ factor will drop out. The same remark applies to the second and the fourth term. As a result, the integrand becomes after some algebra

$$+\frac{2}{s_1(1-\frac{1}{4}s_2^2)}\log\left|\frac{(1+\frac{1}{2}s_1)}{(1-\frac{1}{2}s_1)}\right|$$

and in the limit $R \to 0$ $J(R)$ becomes

$$J(R) = \frac{2}{\pi^2}\int_0^{\pi/2}\frac{\mathrm{d}\phi_2}{1-\frac{1}{4}s_2^2}\int_0^{\pi/2}\frac{\mathrm{d}\phi_1}{s_1}\log\left|\frac{(1+\frac{1}{2}s_1)}{(1-\frac{1}{2}s_1)}\right|$$

and the problem has been reduced to some standard integrals. The integral over ϕ_1 is, using Gradshteyn and Ryzhik (1965) (4.397.1), equal to $\pi^2/6$, while the integral over ϕ_2 equals $\pi/\sqrt{3}$) (using Gradshteyn and Ryzhik (1965) (2.562)). Combining results one finds

$$\lim_{R\to 0} J(R) = \frac{\pi}{3\sqrt{3}}, \tag{A5}$$

a result that agrees with Mori and Janssen (2006). In a similar vein one may consider the large R-limit, and one finds

$$\lim_{R\to\infty} J(R) = -\frac{1}{R}\frac{\pi}{3\sqrt{3}},$$

Furthermore, the only additional analytical result is that for $R = 1$ $J(R)$ indeed vanishes, a finding in agreement with the general result (22).

Thus far we haven't been able to do the integral analytically.[11] Therefore, the integral has been computed on the computer. This was not as straightforward a task as it might seem. A very important element of a succesful

[11] We even tried it with Maxima, but rather then replying that it cannot find the answer it returns the original integral (a strange way of admitting defeat!).

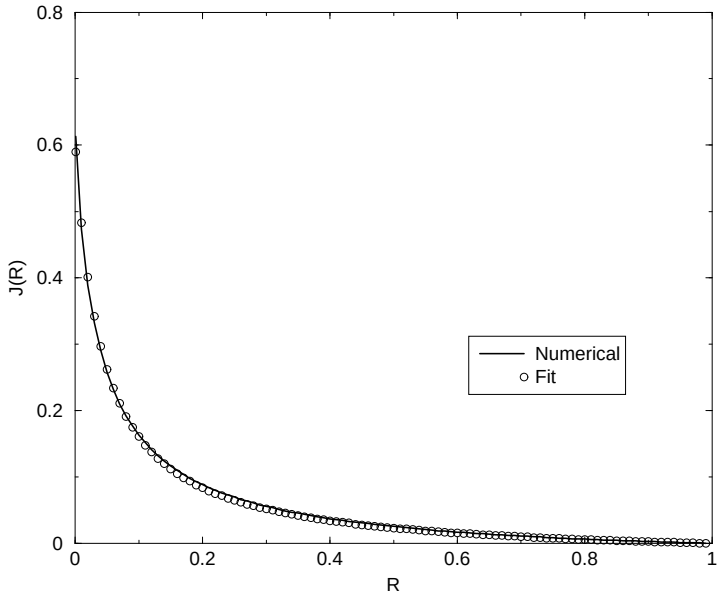

Figure 13: The integral $J(R)$ as function of R for $N = 36$. The parametrization of the integral, labeled with 'Fit' is shown as well.

integration is that the integrand is regularized in the manner prescibed below Eq. (A2). The other important element is that the integration is done over a fixed interval $(\varepsilon, \pi/2)$ with $\varepsilon << 1$. The integrand was discretized in the following manner:

$$\phi_{1,2}^{(n)} = n\Delta\phi + \varepsilon,\ n = 0, N,$$

where $n = N$ corresponds to $\phi_{1,2} = \pi/2$ and $\Delta\phi$ is given by

$$\Delta\phi = \frac{\pi/2 - \varepsilon}{N}.$$

For $N = 36$ the result of the $J(R)$-computation is shown for the range $0 < R < 1$ in Fig. 13. The number of grid points was varied from $N = 18$ to $N = 180$ but the results for $J(R)$ are found to be fairly insensitive to variations in N.

By some trial and error the following fit to the numerical data was tried:

$$J(R) = \frac{1}{(2\pi)^2}\frac{1-R}{R+R_0}, \tag{A6}$$

where $R_0 = 3\sqrt{3}/4\pi^3$. This fit was inspired by the conditions that $J(R)$ should vanish for $R = 1$ while it should reach the limit (A5) for vanishing R. Also, the numerical result suggested that the fit should behave in a hyperbolic fashion, for this reason the denominator. The factor $1/(2\pi)^2$ is unexplained. Nevertheless, the agreement between the numerical results and the fit is impressive.

In order to emphasize the good agreement results of the kurtosis calculation as function of the dimensionless widths δ_ω and δ_θ for a steepness $\varepsilon = 0.1$ are shown in Fig. 14. The right panel shows the fit (A6) where for $R > 1$ the relation $J(R) = -J(1/R)/R$ was used which follows from (21), while the left panel shows the numerical result for $N = 36$. The agreement is more than satisfactory, and it suggests that if spectra are stationary on a long time scale then the fit (A6) is a good candidate for operational implementation of the two-dimensional kurtosis calculation.

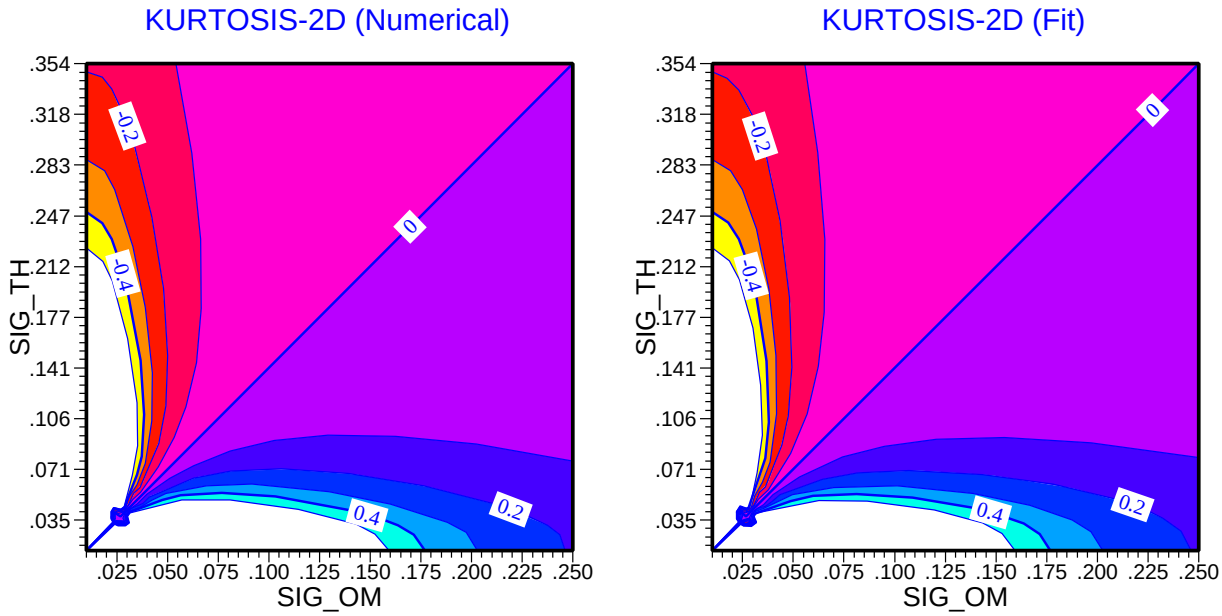

Figure 14: Dependence of kurtosis C_4 on dimensionless frequency width δ_ω and angular width δ_θ for a dimensionless steepness ε of 0.1. The right figure is based on fit (A6) while the left figure is from numerical integrations with $N = 36$.

B Joint distribution of envelope height and period.

B.1 Theory

In order to obtain the joint pdf of envelope and period there is a need to describe a procedure how to obtain from a given time series $\eta(t)$ the envelope ρ and local phase ϕ.

Attention is restricted to analytic functions $Z(t) = \eta + i\xi$. These functions have the remarkable property that if the real part of Z is known then the imaginary part of Z is given by the Hilbert transform of its real part. Thus,

$$\xi = \Im(Z) = \pm H(\eta) = \pm\frac{1}{\pi}\int \mathrm{d}\tau \frac{\eta(\tau)}{t-\tau}, \tag{B1}$$

where the integral is a principle value integral and the $\pm$ sign depends on the chosen assumed behaviour of the complex function Z for large arguments (cf. remark below). Envelope ρ and phase ϕ are now defined as

$$\rho\, e^{i\phi} = Z(t) = \eta + i\xi,$$

therefore

$$\eta = \rho\cos\phi,\ \xi = \rho\sin\phi. \tag{B2}$$

Envelope and phase follow now at once from η and ξ,

$$\rho = \sqrt{\eta^2+\xi^2},\ \phi = \arctan(\xi/\eta). \tag{B3}$$

In this fashion (and this is of course very well-known) one may obtain from a real time series envelope and phase of a wave train. This is a very general approach. For a narrow-band wave train (but note that this assumption

will not be made here) ρ will be a slowly varying function in time and space. In those circumstances it is costumary to introduce the local angular frequency through

$$\omega = -\frac{\partial \phi}{\partial t}, \tag{B4}$$

and for a narrow-band wave train the local frequency is also slowly varying. The key-point is now that the notion of a local frequency is generalized by applying the same definitions also for a wave train with a broad-banded spectrum. Hence, for any time series η envelope and phase are obtained from Eq. (B3) where ξ is the Hilbert transform of η. The joint pdf of envelope ρ and period T is then easily obtained by making use of the local frequency ω of Eq. (B4) and the definition $T = 2\pi/\omega$.

Remarks on the procedure

It is indeed a remarkable result that one may construct a complex signal Z from its real part and the Hilbert transform of its real part, but there is also a caveat. A unique solution can only be found provided one makes an assumption regarding the behaviour of the complex function $Z(z)$ for large complex z.

It is quite amazing that given a function $g(x)$ on the real axis, it is possible to find a unique analytical function $f(z) = g(z) + ih(z)$, where $z = x + iy$. This is simply not possible unless some conditions on the behaviour of $f(z)$ for large z are imposed. To illustrate the point consider the function $g(x) = \cos x$. There are at least two complex functions $f(z)$ that give the same function on the real axis, namely $f(z) = \exp(iz)$ and $f(z) = \exp(-iz)$. So the solution is not unique unless one imposes an additional condition on the behaviour of $f(z)$. Imposing the condition that $f(iy)$ vanishes sufficiently rapidly for $y \to \infty$ will give rise to the unique solution $f(z) = \exp(iz)$, while the condition that $f(iy)$ will vanish sufficiently rapidly for $y \to -\infty$ will give rise to the second solution $f(z) = \exp(-iz)$.

This has consequences for the extension of a real signal in the complex domain. In order to show this start from the Cauchy theorem. Consider an integral in the complex z-plane of the form

$$\int_C \frac{f(z)}{z - z_0} \mathrm{d}z,$$

If $f(z)$ is analytic and C is a piecewise smooth closed contour in an open domain, then according to the Cauchy integral theorem

$$\int_C \frac{f(z)}{z - z_0} \mathrm{d}z = 2\pi i f(z_0),$$

if z_0 is inside C. If z_0 is outside C then the singular integral vanishes.

The result in Eq. (B1) now follows by making a special choice of the contour C. Consider a contour C that consists of a semicircle Γ_R with radius R and the real axis from $-R$ to $+R$, hence $C = \Gamma_R + [-R, R]$. First suppose that $f(z)$ vanishes sufficiently rapidly for $y \to \infty$ so that the contribution from the semicircle in the upper half-plane, Γ_R^u vanishes. In the limit $R \to \infty$ one then finds

$$P \int_{-\infty}^{\infty} \frac{f(\xi)}{\xi - x} \mathrm{d}z = \pi i f(x),$$

Writing $f(x) = g(x) + ih(x)$ one immediately finds from the real part of the above equation that

$$h(x) = \frac{1}{\pi} P \int_{-\infty}^{\infty} \frac{g(\xi)}{x - \xi} \mathrm{d}z.$$

corresponding to the $+$ sign result of Eq. (B1).

However, if one now assumes on the other hand that $f(z)$ vanishes sufficiently rapidly for $y \to -\infty$ then in order that the contribution along the semicircle vanishes one has to close the contour C by choosing a semicircle Γ_R^l in the lower half-plane. The end result is a $-$ sign difference as

$$h(x) = -\frac{1}{\pi} P \int_{-\infty}^{\infty} \frac{g(\xi)}{x - \xi} \mathrm{d}z.$$

Therefore the extension of a real function into the complex plane is not unique, and results will depend on assumptions regarding the behaviour of the complex function for large z.

In order to obtain the joint pdf of envelope and period the work of Longuet-Higgins (1983) is followed, with corrections provided by Xu *et al.* (2004). Starting point is the assumption that $\eta(t)$ is a stationary Gaussian process. Since $\dot{\eta}$, ξ and $\dot{\xi}$ are linear transforms of η their joint pdf is gaussian and therefore can be expressed as

$$p(\mathbf{x}) = \frac{1}{(2\pi)^2|\Sigma|^{1/2}} \exp\left\{-\frac{1}{2}\mathbf{x}^T\Sigma^{-1}\mathbf{x}\right\},$$

where $\mathbf{x} = (\eta, \xi, \dot{\eta}, \dot{\xi})$, and the covariance matrix is given by $\Sigma_{ij} = \langle x_i x_j \rangle$. Fortunately, a number of elements in the correlation matrix Σ vanish, and the elements with a finite value are:

$$\Sigma_{11} = \Sigma_{22} = m_0,\ \Sigma_{14} = \Sigma_{41} = -m_1,\ \Sigma_{23} = \Sigma_{32} = m_1,\ \Sigma_{33} = \Sigma_{44} = m_2.$$

With this choice of Σ the determinant $|\Sigma|$ becomes

$$|\Sigma| = \Delta^2,\ \Delta = m_0 m_2 - m_1^2,$$

and the joint pdf becomes

$$p(\mathbf{x}) = \frac{1}{(2\pi)^2\Delta} \exp\left\{-\frac{1}{2\Delta}\left[m_2(\eta^2+\xi^2) + m_0(\dot{\eta}^2+\dot{\xi}^2) - 2m_1(\xi\dot{\eta} - \eta\dot{\xi})\right]\right\}.$$

From this the joint pdf of $\rho, \phi, \dot{\rho}, \dot{\phi}$ is found by the usual transformation rule, i.e.

$$p(\rho, \phi, \dot{\rho}, \dot{\phi}) = p(\mathbf{x})\, J,$$

where the Jacobian $J = \partial(\eta, \xi, \dot{\eta}, \dot{\xi})/\partial(\rho, \phi, \dot{\rho}, \dot{\phi})$ follows from the transformation given in Eq. (B2). One finds $J = \rho^2$, and the joint pdf becomes

$$p(\rho, \phi, \dot{\rho}, \dot{\phi}) = \frac{\rho^2}{(2\pi)^2\Delta} \exp\left\{-\frac{1}{2\Delta}\left[m_2\rho^2 + m_0(\dot{\rho}^2 + \rho^2\dot{\phi}^2) + 2m_1\rho^2\dot{\phi}\right]\right\}. \tag{B5}$$

The joint pdf of ρ and $\dot{\phi}$ is then found by integrating Eq. (B5) over $\dot{\rho}$ from $-\infty$ to $+\infty$ and over ϕ from 0 to 2π. The result is

$$p(\rho, \dot{\phi}) = \frac{\rho^2}{\sqrt{2\pi m_0}\Delta} \exp\left\{-\frac{\rho^2}{2\Delta}\left(m_2 + m_0\dot{\phi}^2 + 2m_1\dot{\phi}\right)\right\}.$$

Finally, it is then straightforward to obtain the joint pdf of normalized envelope,

$$R = \frac{\rho}{\sqrt{2m_0}},$$

and normalized period

$$T = \frac{\tau}{\bar{\tau}},$$

where the period $\tau = 2\pi/\omega = -2\pi/\dot{\phi}$, and the mean period $\overline{\tau} = 2\pi m_0/m_1$. The eventual result is

$$p(R,T) = \frac{2}{\nu\pi^{1/2}}\frac{R^2}{T^2}\exp\left\{-R^2\left[1+\frac{1}{\nu^2}\left(1-\frac{1}{T}\right)^2\right]\right\}, \tag{B6}$$

where ν is the width parameter as introduced by Longuet-Higgins (1983),

$$\nu = (m_0 m_2/m_1^2 - 1)^{1/2}.$$

There are two marginal distribution laws. The first one is the pdf of the envelope and is obtained by integration over period T. The result is

$$p(R) = 2R\,e^{-R^2}, \tag{B7}$$

hence the envelope R follows the *Rayleigh* distribution, independent of the width of the spectrum. The second marginal distribution law is the pdf of the period, and is obtained by integration over the envelope with the result

$$p(T) = \frac{1}{2\nu T^2}\left[1+\frac{1}{\nu^2}\left(1-\frac{1}{T}\right)^2\right]^{-3/2}, \tag{B8}$$

which shows, as to be expected, a sensitive dependence on the width of the spectrum.

Comments

1 Longuet-Higgins (1983) derived the joint pdf for envelope and period by considering only positive periods T. Ignoring negative periods will result in an envelope distribution which shows slight deviations from the Rayleigh statistics. However, for finite band-width spectra there is a finite but small probability that periods become negative. Including these negative periods, as done here will then result in the Rayleigh distribution for the envelope (see Xu *et al.*, 2004).

2 Xu *et al.* (2004) claim that there is an additional multiplicative factor in the joint pdf of envelope and period. Presumably this is connected to their definition of wave period $\tau = 2\pi/|\omega|$ which involves the absolute value of $\dot{\phi}$. Their definition differs from the present one, as here negative frequencies and periods are allowed reflecting the fact that waves may propagate to the right or to the left.

B.2 Monte Carlo simulations

In order to show the general validity of the result (B6) Monte Carlo simulations have been performed for linear wave trains. Introduce the complex representation Z of a train of surface gravity waves

$$Z(t) = \sum_k a_k e^{-i(\omega_k t+\theta_k)}, \tag{B9}$$

where $\omega_k = (gk)^{1/2}$ is the dispersion relation for surface gravity waves, θ_k is a randomly chosen phase, and a_k is drawn from a given wavenumber spectrum with peak wavenumber $k_p = 1$ using a Rayleigh distribution. Two discretisations of the wave number haven been chosen, namely a linear grid,

$$k = \alpha\, n,\ n = 0, N$$

where $N+1$ is the number of wave components and α is a fraction of the width σ_k of the spectrum (typically $\alpha = 0.025\sigma_k$ and $N = 100$), and a logarithmic grid

$$k = k_0(1+\alpha)^n,\ n = 0, N$$

where k_0 is the start wave number (typically $k_0 = 0.1$, and $\alpha = 0.7\sigma_k$).

The surface elevation η given by

$$\eta = \frac{1}{2}(Z + Z^*)$$

can then be shown to follow a Normal distribution.

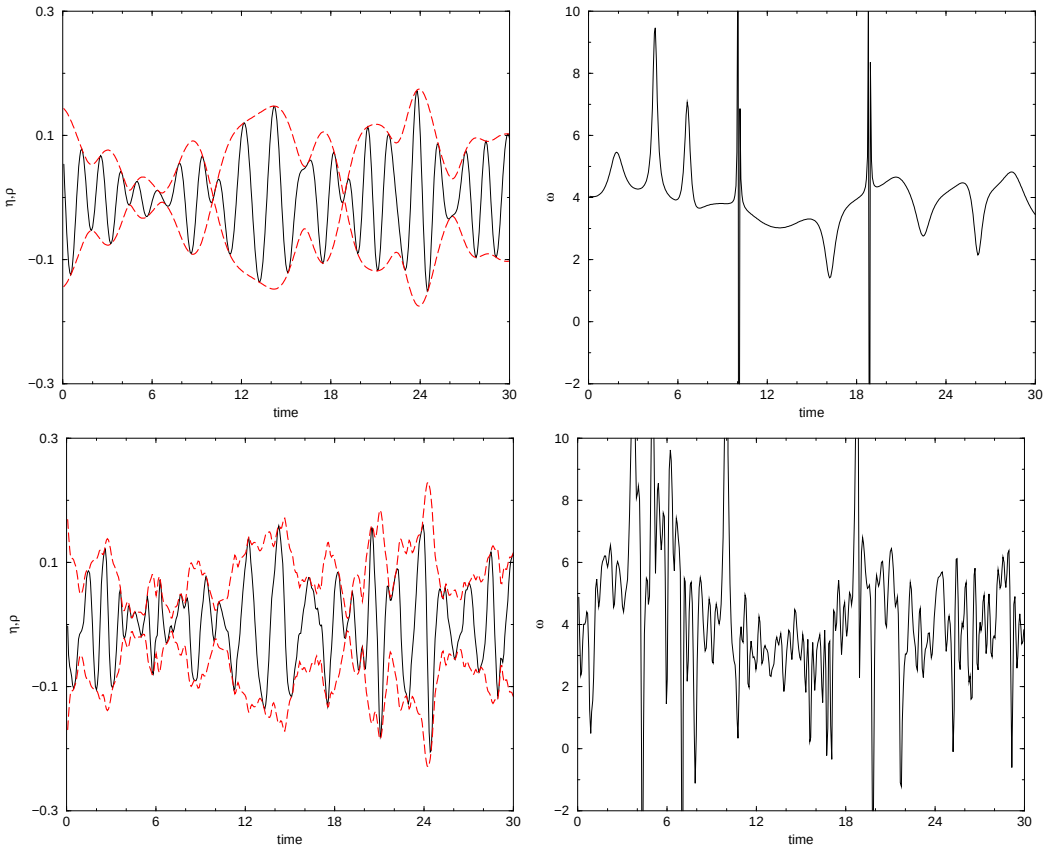

Figure 15: Envelope ρ and local frequency ω for a narrow-band (top, $\nu = 0.24$) and a broad-band (bottom, $\nu = 0.40$) signal.

The complex function Z of Eq. (B9) has the property that it vanishes for $\Im(t) \to -\infty$, hence in order to determine the auxiliary variable ξ I take the minus sign in Eq. (B1). Hence,

$$\xi = -H(\eta), \tag{B10}$$

and since it is straightforward to show that

$$H(e^{-i\omega_k t}) = ie^{-i\omega_k t},$$

one finds

$$\xi = -\frac{i}{2}(Z - Z^*).$$

Therefore, in the context of a linear wave solution with constant amplitudes a_k it is straightforward to obtain the auxiliary variable ξ, using the Hilbert transform. It is remarkable, that the pair (η, ξ) just corresponds to the canonical variables of the Hamiltonian formulation of water waves.

Using (B10) and (14) envelope ρ and phase ϕ follow from Eq. (B3) while the local frequency follows from Eq. (B4). For the Pierson-Moskowitz spectrum on the logarithmic grid an example of results for envelope and local frequency is shown in Fig. 15. Shown are two cases. The first case is a Pierson-Moskowitz spectrum where the spectrum is cut-off at twice the peak frequency, giving a spectral width $\nu = 0.24$,, while the second case has the cut-off at 8 times the peak frequency, which gives $\nu = 0.40$. It is evident that the broad-band spectrum gives a more erratic behaviour in time of the envelope and the local frequency. In addition, note the occasional occurrence of negative local frequencies.

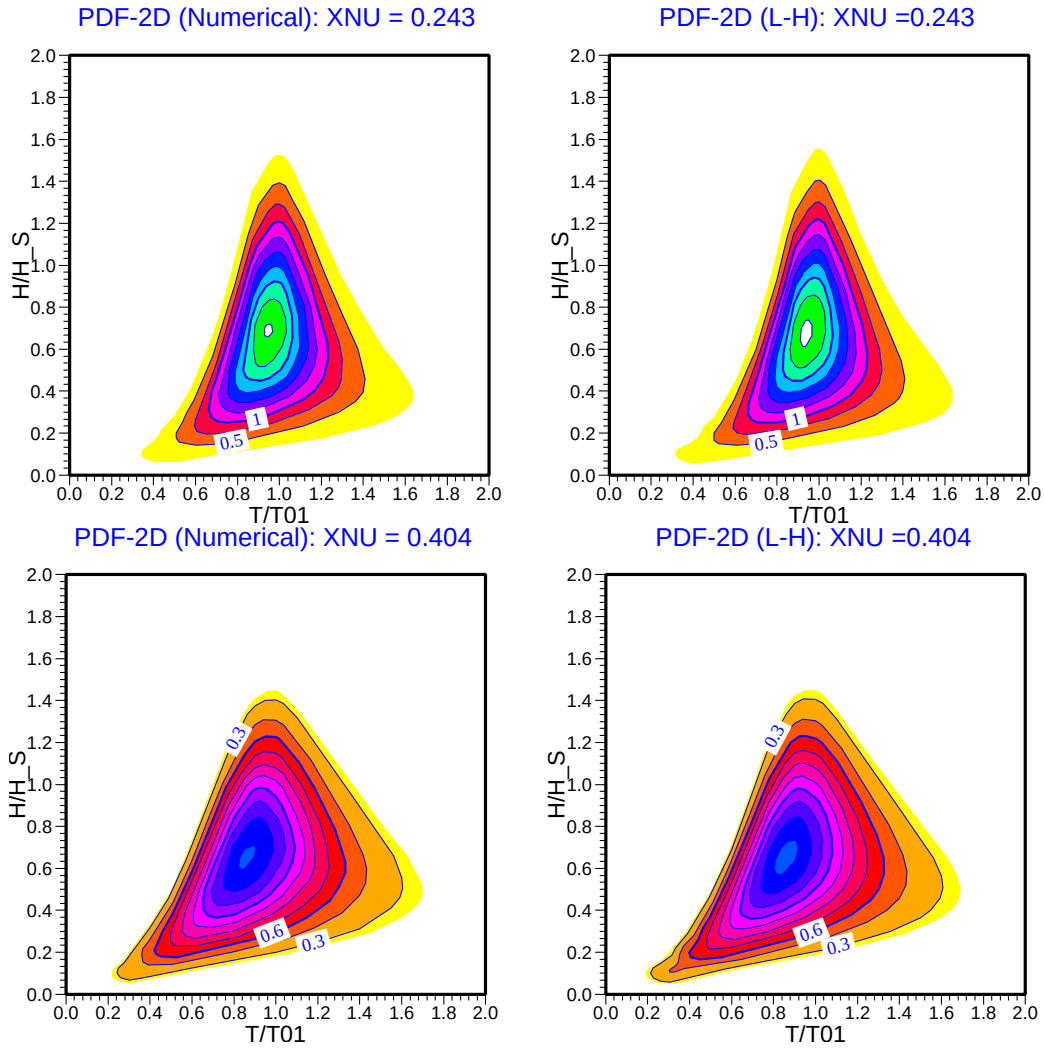

Figure 16: Joint pdf of envelope wave height H/H_S (with $H = 2\rho$) and period $T/T01$ for a narrow-band (top, $\nu = 0.24$) and a broad-band (bottom, $\nu = 0.40$) case. For comparison the theoretical distribution is shown as well.

Fig. 16 shows for the same two cases a comparison of the theoretical joint pdf of envelope wave height and period with the numerical simulation. The agreement is almost perfect, even for the broad band case. In order to simulate the pdf η and ξ have been calculated for a 100 member ensemble and each timeseries was 1000 wave periods long. The pdf was determined by counting the number of times the envelope wave height 2ρ and local period T entered a certain wave-height, period bin.

Finally, Fig. (17) shows for the broad-band case only a comparison of the numerically simulated marginal distribution laws with the theoretically ones, given in (B7) and (B8)

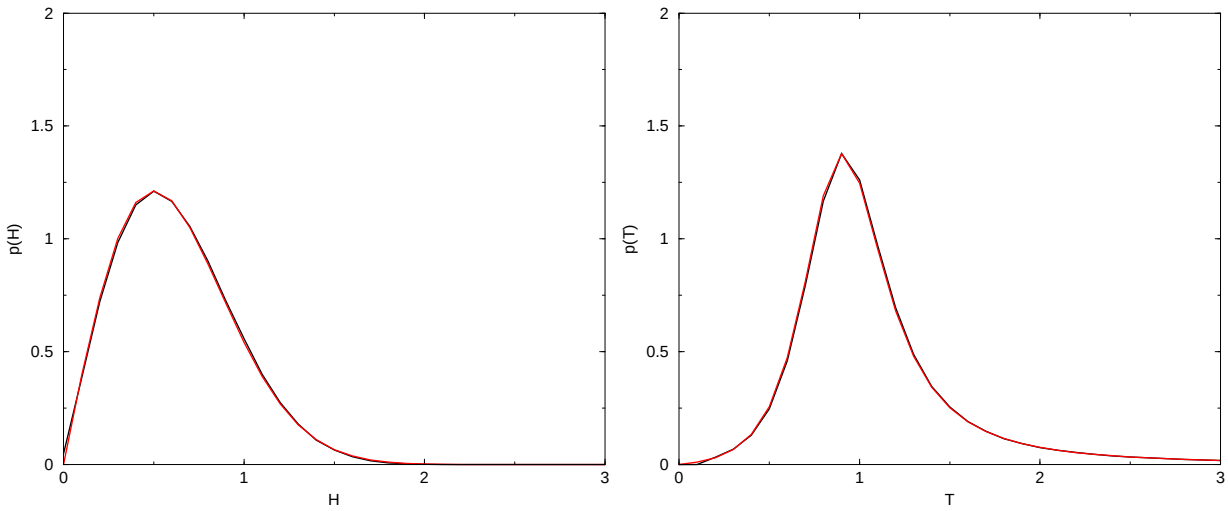

Figure 17: Comparison of simulated (black) and theoretical (red) marginal distribution laws for envelope wave height and period. The spectrum corresponds to the broad-band case ($\nu = 0.40$).

It is concluded that there is good agreement between the theoretical probability distributions and the results obtained with Monte Carlo simulations. This implies that the time series analysis here, which is based on the simple description that $\eta = \rho \cos \phi$, where the local frequency follows from the time derivative of the phase, seems to work, even for broad-banded spectra.

C Evaluation of Eq. (31) and additional results.

The maximum wave height distribution becomes explicitely

$$p(y) = 4Nye^{-2y^2}\left[1+C_4A_H(y)\right]e^{-Ne^{-2y^2}\left[1+C_4B_H(y)\right]}, \tag{C1}$$

where $A_H = 2y^4 - 4y^2 + 1$ and $B_H = 2y^2\left(y^2-1\right)$, illustrating that the maximum wave height distribution is indeed a double exponential. For analysis purposes it is more convenient to introduce the parameter z,

$$z = y^2$$

and to introduce the function

$$\mathscr{G}(z) = -Ne^{-2z}\left(1+C_4B\right),\ B = 2z\left(z-1\right). \tag{C2}$$

Then the maximum wave height distribution assumes the simple form

$$p(z) = \frac{\mathrm{d}\mathscr{G}}{\mathrm{d}z}\exp(\mathscr{G}). \tag{C3}$$

Now quantities such as the expectation value of y and the width σ of the distribution are evaluated. Anticipating that the width σ of the distribution function (C3) is small, $\langle y\rangle$ is determined by means of the approximation $\langle y\rangle \simeq \langle z\rangle^{1/2}$, and afterwards it is shown that σ is indeed small. The expectation value of $\langle z\rangle$ can be found in the limit of large N and small C_4 in the following manner. By definition

$$\langle z\rangle = \int_0^\infty \mathrm{d}z\, zp(z).$$

Changing from integration variable z to $x = -\mathscr{G}$ gives

$$\langle z\rangle = \int_0^N \mathrm{d}x\, z(x)e^{-x}. \tag{C4}$$

and $z = z(x)$ is obtained by solving the relation between x and z, i.e.

$$x = Ne^{-2z}\left(1+C_4B(z)\right)$$

with a perturbation approach. Take the log and rearrange, then

$$z = \frac{1}{2}\log\left(\frac{N}{x}\right) + \frac{1}{2}\log\left(1+C_4B(z)\right)$$

and for small C_4 one finds in good approximation

$$z = z_0 + \frac{1}{2}\log\left(1+C_4B(z_0)\right),\ z_0 = \frac{1}{2}\log\left(\frac{N}{x}\right) \tag{C5}$$

As a consequence, using (C5) in (C4) gives

$$\langle z\rangle = \int_0^N \mathrm{d}x\,\left[z_0 + \frac{1}{2}\log\left(1+C_4B(z_0)\right)\right]e^{-x} = z_1 + z_2 \tag{C6}$$

Consider the first integral

$$z_1 = \int_0^N \mathrm{d}x\, z_0e^{-x} = \frac{1}{2}\int_0^N \mathrm{d}x\, e^{-x}\left(\log N - \log x\right) = \frac{1}{2}\log N - \frac{1}{2}\int_0^N \mathrm{d}x\, e^{-x}\log x$$

The second integral turns out to be relatively small. It is connected to the exponential integral $\mathrm{Ei}(x)$ and to the logarithm of the Gamma function $\Gamma(z)$. According to Gradshteyn and Ryzhik (1965) one has

$$\int_0^N \mathrm{d}x\, e^{-x} \log x = \mathrm{Ei}(x) - \gamma - e^{-N} \log N$$

where $\gamma = 0.5772$ is Euler's constant and

$$\mathrm{Ei}(-x) \sim e^{-x} \sum_{k=1}^{\infty} (-1)^k \frac{(k-1)!}{x^k} = \mathscr{O}(\frac{e^{-N}}{N}) \to 0.$$

Hence, apart from exponentially small terms one finds

$$\int_0^N \mathrm{d}x\, e^{-x} \log x = -\gamma$$

and therefore

$$z_1 = \frac{1}{2}(\log N + \gamma)$$

Consider now the second integral in (C6),

$$z_2 = \frac{1}{2} \int_0^N \mathrm{d}x\, \log\left[1 + C_4 B(z_0)\right] e^{-x}$$

Utilizing once more the assumption that C_4 is small the logarithm is expanded. Elimination of z_0 and rearrangement then gives

$$z_2 = \frac{C_4}{2} \left\{ 2\hat{z}_0(\hat{z}_0 - 1) + (1 - 2\hat{z}_0) \int_0^{\infty} \mathrm{d}x\, e^{-x} \log x - \frac{1}{2} \int_0^{\infty} \mathrm{d}x\, e^{-x} \log^2 x \right\}$$

where $\hat{z}_0 = \frac{1}{2} \log N$, and the upper bound N is replaced by ∞ as this only introduces an exponentially small term. Integrals involving exponentials and logarithms are related to the Gamma function $\Gamma(z)$ and its derivatives,

$$\Gamma(1+z) = \int_0^{\infty} t^z e^{-t} \mathrm{d}t = \int_0^{\infty} e^{z \log t} e^{-t} \mathrm{d}t,$$

and therefore

$$\left.\frac{\mathrm{d}}{\mathrm{d}z}\Gamma\right|_{z=0} = \int_0^{\infty} \log t\, e^{-t} \mathrm{d}t,$$

$$\left.\frac{\mathrm{d}^2}{\mathrm{d}z^2}\Gamma\right|_{z=0} = \int_0^{\infty} \log^2 t\, e^{-t} \mathrm{d}t.$$

It may be shown that $\Gamma'(1) = -\gamma$, and $\Gamma''(1) = \gamma^2 + \frac{\pi^2}{6}$. Now, returning to the logarithmic form one finds for z_2

$$z_2 = \frac{1}{2} \log \left[1 + \frac{C_4}{2} \left\{ 2\hat{z}_0(\hat{z}_0 - 1) - \gamma(1 - 2\hat{z}_0) - \frac{1}{2}(\gamma^2 + \frac{\pi^2}{6}) \right\} \right].$$

Finally, combining the results for z_1 and z_2 one finds for $\langle z \rangle$

$$\langle z \rangle = \hat{z}_0 + \frac{\gamma}{2} + \frac{1}{2} \log \left[1 + \frac{C_4}{2} \left\{ 2\hat{z}_0(\hat{z}_0 - 1) - \gamma(1 - 2\hat{z}_0) - \frac{1}{2}(\gamma^2 + \frac{\pi^2}{6}) \right\} \right],$$

with $\hat{z}_0 = \frac{1}{2}\log N$, while the expectation value of H_{max} is given by $\langle z\rangle^{1/2}$. The analytical result has been compared with results of numerical computations of $\langle H_{max}\rangle$ and the agreement is astonishingly good. Notice that the assumption has been made that the kurtosis is small, in agreement with the assumptions on weakly nonlinear waves. Therefore, in the operational model, when $\langle H_{max}\rangle$ is computed, the kurtosis is resticted to the range $-0.33 < C_4 < 1$.

Next, a sketch is given of how the width σ of the maximum wave height distribution has been obtained. By definition

$$\langle z\rangle = \sigma^2 + \langle z^{1/2}\rangle^2,$$

therefore the expectation value of H_{max} denoted by $\langle z^{1/2}\rangle$ and defined as

$$\langle z^{1/2}\rangle = \int_0^N \mathrm{d}x\, z^{1/2} e^{-x} = \frac{1}{\sqrt{2}} \int_0^N \mathrm{d}x\, e^{-x} \sqrt{(\log N - \log x) + C_4 B(z_0)}$$

is needed. This integral can be evaluated for large N and small C_4. In particular a Taylor expansion of the square root term is performed where the $\log N$-term is the dominant term. Although for large x the $\log x$ term is of a similar magnitude, the contributions for large x to the integral are exponentially small because of the exponential. The integrations can then be performed in a similar fashion as before, and for linear waves (i.e. $C_4 = 0$) the relative width $\sigma/\langle H_{max}\rangle$ becomes

$$\frac{\sigma}{\langle H_{max}\rangle} \simeq \frac{\pi}{2\sqrt{6}\left(\log N + \frac{1}{2}\gamma\right)}.$$

For typical choices of the number of waves, $N = 1000$, the relative width is found to be around 9%. The difference between $\langle z\rangle^{1/2}$ and $\langle z^{1/2}\rangle$ then turns out to be less than 1%. In this sense the maximum wave height distribution is narrow, allowing a meaningful comparison with observations as described in the main text.

From the pdf of H_{max} it is possible to obtain random draws of maximum wave height using the cumulative distribution, defined as

$$P(y) = \int_0^y \mathrm{d}y\, p(y) = \int_0^z \mathrm{d}z\, p(z)$$

where once more $z = y^2$ is introduced. Making use of the form of the pdf given in Eq. (C3) the integration can be performed with the result

$$P(y) = e^{\mathscr{G}(z)} - e^{\mathscr{G}(0)} = e^{\mathscr{G}(z)} - e^{-N}$$

where $\mathscr{G}(z)$ is given in (C2), and $\mathscr{G}(0) = -N$. Now $P(y)$ is in the range of 0 to 1 and the random draw of z follows from the inverse cumulative distribution

$$\mathscr{G}(z) = \log(P(y) + e^{-N}) = \log(r + e^{-N}),$$

where r is drawn from the uniform distribution (0,1). An explicit expression for z is now obtained by an iteration process that is identical to the one used for evaluating the integrals in the beginning of this Appendix. Hence, write $\mathscr{G}(z) = \mathscr{G}_0(z)\mathscr{G}_1(z)$ where $\mathscr{G}_0(z) = -N\exp(-2z)$ and $\mathscr{G}_1(z) = 1 + C_4 B(z)$, then the random draw for z, denoted by z_r, is approximately given by

$$z_r = -\frac{1}{2}\log\left(-\frac{\log(r + e^{-N})}{N\mathscr{G}_1(z_0)}\right),$$

where $z_0 = -0.5\log\left(-\log(r + e^{-N})/N\right)$. Note that the exponentially small term e^{-N} needs to be retained because otherwise z_r might become negative. The random draw for normalised H_{max} then follows from $H_{max} = \sqrt{z_r}$.

References

Benjamin, T.B., and J.E. Feir, 1967. The disintegration of wavetrains on deep water. Part 1. Theory. *J. Fluid Mech.* **27**, 417-430.

Bidlot J.-R., P.A.E.M. Janssen, and S. Abdalla, 2005: On the importance of spectral wave observations in the continued development of global wave models. *Proc. Fifth Int. Symposium on Ocean Wave Measurement and Analysis WAVES2005*, 3rd-7th July 2005, Madrid, Spain.

Bidlot J.-R., J.-G. Li, P. Wittmann, M. Faucher, H. Chen, J.-M, Lefevre, T. Bruns, D. Greenslade, F. Ardhuin, N. Kohno, S. Park and M. Gomez, 2007: Inter-Comparison of Operational Wave Forecasting Systems. *Proc. 10th International Workshop on Wave Hindcasting and Forecasting and Coastal Hazard Symposium*, North Shore, Oahu, Hawaii, November 11-16, 2007.

Burgers, G., F. Koek, H. de Vries and M. Stam, 2008. Searching for factors that limit observed extreme maximum wave height distributions in the North Sea. *Extreme Ocean Waves*, E. Pelinovsky and C. Kharif (eds), Springer Science+Business Media B.V., pp. 127-138.

Crawford, D.R., B.M. Lake, P.G. Saffman and H.C. Yuen, 1981. Stability of weakly nonlinear deep-water waves in two and three dimensions. *J. Fluid Mech.* **105**, 177-191.

Dean, R.G., 1990. Freak waves: A possible explanation. In A. Torum & O.T. Gudmestad (Eds.), *Water Wave Kinematics* (pp. 609-612), Kluwer.

Draper, L., 1965. 'Freak' ocean waves. *Marine Observer* **35**, 193-195.

Gradshteyn, I.S. and I.M. Ryzhik, 1965. Tables of integrals, series, and products, Academic Press Inc, New York and London.

Hasselmann, S., K. Hasselmann, J.H. Allender and T.P. Barnett, 1985. Computations and parameterizations of the nonlinear energy transfer in a gravity wave spectrum, part 2: Parameterizations of the nonlinear energy transfer for application in wave models. *J. Phys. Oceanogr.* **15**, 1378-1391.

Janssen, P.A.E.M., 2003. Nonlinear Four-Wave Interactions and Freak Waves. *J. Phys. Oceanogr.* **33**, 863-884.

Janssen, P.A.E.M., 2008. Some consequences of the canonical transformation in the Hamiltonian theory of water waves, to be published.

Janssen, P.A.E.M., and E. Bouws, 1986. On the minimum width of a gravity wave spectrum, KNMI-OO Memorandum OO-86-01, KNMI, De Bilt, The Netherlands.

Janssen, P.A.E.M., and M. Onorato, 2007. The Intermediate Water Depth Limit of the Zakharov Equation and Consequences for Wave Prediction. *J. Phys. Oceanogr.* **37**, 2389-2400.

Kimura, A., 1980. Statistical properties of random wave groups. *Proc. 17th Int. Conf. on Coastal Engng, Sydney*, pp. 2955-2973. New York: Am. Soc. Civ. Engrs.

Lake B.M., H.C Yuen, H. Rungaldier, and W.E. Ferguson, 1977. Nonlinear deep-water waves: Theory and experiment. Part 2. Evolution of a continuous wave train, *J. Fluid Mech.* **83**, 49-74.

Longuet-Higgins, M.S., 1957. The statistical analysis of a random, moving surface, *Phil. Trans. R. Soc. Lond.* **A 249**, 321-387.

Longuet-Higgins, M.S., 1983. On the joint distribution of wave periods and amplitudes in a random wave field. *Proc. Roy. Soc. London* **A389**, 241-258.

Longuet-Higgins, M.S., 1984. Statistical properties of wave groups in a random sea state. *Phil. Trans. R. Soc. Lond.* **A312**, 219-250.

Mori N. and P.A.E.M. Janssen, 2006. On kurtosis and occurrence probability of freak waves. *J. Phys. Oceanogr.* **36**, 1471-1483.

Nobuhito Mori, Miguel Onorato, Peter A. E. M. Janssen, Alfred R. Osborne, and Marina Serio, 2007. On the extreme statistics of long-crested deep water waves: Theory and experiments, *J. Geophys. Research* **112**, 3351,doi:10.1029/2006JC004024, 10 pp.

Onorato, M., T. Waseda, A. Toffoli, L. Cavaleri, O. Gramstad, P.A.E.M. Janssen, T. Kinoshita, J. Monbaliu, N. Mori, A.R. Osborne, M. Serio, C.T. Stansberg, H. Tamura, and K. Trulsen, 2009. Statistical properties of directional ocean waves: the role of the modulational instability in the formation of extreme events. *Phys. Rev. Lett.* **102**, 114502/1-4.

Osborne, A.R., M. Onorato, and M. Serio, 2000. The nonlinear dynamics of rogue waves and holes in deep water gravity wave trains. *Phys. Lett. A* **275**, 386-393.

Rice, S.O., 1945. The mathematical analysis of random noise. *Bell Syst. Tech. J.* **24**, 46-156.

Stansell, P., 2005. Distributions of extreme wave, crest and trough heights measured in the North Sea. Ocean Engineering **32**, 1015-1036.

Trulsen K., and K. Dysthe, 1997. Freak Waves-A Three-dimensional Wave Simulation. in *Proceedings of the 21st Symposium on naval Hydrodynamics*(National Academy Press), pp 550-558.

Uhlenbeck, G.E., 1943. Theory of random process. M.I.T. Radiation Lab. Rep. 454, October 1943.

Waseda, T. 2006. Impact of directionality on the extreme wave occurrence in a discrete random wave system. In Proc. 9th Int. Workshop on Wave Hindcasting and Forecasting. Victoria, Canada.

Wolfram J., and B. Linfoot, 2000. Some experiences in estimating long and short term statistics for extreme waves in the North Sea. Abstract for the *Rogue waves 2000 workshop*, Ifremer, Brest.

Xu D., X. Li, L. Zhang, N. Xu, and H. Lu, 2004. On the distributions of wave periods, wave lengths and amplitudes in a random wave field, *J. Geophys. Res.* **109**, C05016,doi:10.1029/2003JC002073.

Yasuda, T., N. Mori, and K. Ito, 1992. Freak waves in a unidirectional wave train and their kinematics. *Proc. 23rd Int. Conf. on Coastal Engineering*, Vol. 1, Venice, Italy, American Society of Civil Engineers, 751-764.

Zakharov, V.E., 1968. Stability of periodic waves of finite amplitude on the surface of a deep fluid. *J. Appl. Mech. Techn. Phys.* **9**, 190-194.